International Journal of Mechanical Sciences 205 (2021) 106573

Contents lists available at ScienceDirect

International Journal of Mechanical Sciences

journal homepage: www.elsevier.com/locate/ijmecsci

Tuning of topological interface modes in an elastic beam array system with inerters

Milan Cajić [a,b,*], Johan Christensen [c], Sondipon Adhikari [a]

[a] College of Engineering, Swansea University, Swansea SA1 8EN, United Kingdom
[b] Mathematical Institute of the Serbian Academy of Sciences and Arts, Kneza Mihaila 36, Belgrade 11000, Serbia
[c] Department of Physics, Universidad Carlos III de Madrid, Leganès, Madrid ES-28916, Spain

ARTICLE INFO

Keywords:
Inerter
Elastic beam array
Interface modes
Band transition
Topological insulators

ABSTRACT

Topological phononic crystals in the mechanical setup became a topic of great interest owing to their applicability in various engineering systems such as waveguides or vibration isolation devices. If such systems are composed of elastic structures, they are usually characterized by a bulk-edge correspondence where the geometrical and material properties can play important role in the existence of stable surface and boundary modes. This work investigates the band transition and topological interface modes in a beam array system, where two sub-lattices of vertically aligned, parallel, and elastically coupled beams are connected at the chain center. To illustrate the existence of interface modes and understand their behavior, the corresponding eigenvalue problem is solved and frequency response function is sought for the system with a finite number of unit cells. Localization of the interface modes is demonstrated based on the steady-state responses of the beam array system to harmonic excitation. The effects of introduced defect masses and inerters on interface states are studied separately. It is revealed that the introduction of a small defect mass in the form of concentrated mass attached to some beam in the system does not affect the interface modes within the observed frequency range. On the other side, inerters produce frequency shifts towards lower values, which even in the case of small values of the inerter parameter causes the interface modes to vanish or even to appear inside another frequency band gap. The obtained results give an insight into the influence of inerter devices and their mass amplification effect on the interface states in complex periodic elastic systems. It also investigates the possibility to tune interface modes without significantly affecting the main band structure properties of the system.

1. Introduction

The most common components of engineering systems are periodic structures, whose understanding of the dynamic behaviour or wave propagation properties is often the most important step in achieving their functionality. Such systems can be designed to achieve unique elastic wave characteristics [1], where many ideas come from condensed matter physics and investigations in the field of photonic and phononic crystals or acoustic metamaterials [2]. Probably the most intriguing is an application of quantum spin Hall effects and other topological concepts [3–5] in acoustics and elasticity. Many studies paid attention to topologically protected interface modes in 1D phononic crystals [6] and patterned elastic structures [7] that are immune to defects and exhibit scattering-free wave propagation. Based on their geometric properties, periodic structures can be classified as one-, two- or three-dimensional ones, whose topological properties of wave modes can be determined through topological invariants such as Berry phase [8] or its special case called Zak phase [9,10]. As given in [11,12], the Berry phase is a geometric phase defined as the integration of Berry connection along a closed-loop inside the Brillouin zone (BZ). Therefore, the key thing in the emergence of interface modes in phononic crystals is the geometric phases and wave mode polarization defined by the type of symmetry of edge-mode state, which is the property that can be proved based on experiments and fundamental 1D or more complex 2D and 3D models of acoustic [13–15] and elastic systems [16–18]. Some authors [19] made a connection between the surface impedance of a one-dimensional PC and its Zak phases of the bulk bands to determine the existence of interface states in particular band gaps. This methodology was later applied to determine topological interface states in multiple bands photonic crystals [20], one-dimensional labyrinthine acoustic metamaterials [21] and translational metamaterials [22]. Another but similar approach relies on the determination of topological invariants named winding numbers [23,24] representing eigenvectors around the origin of the complex plane. Marques et al. [25] proposed the generalization of the Zak phase for lattice models with a non-centered inversion symmetry axis by adding the appropriate correction term. Based on the Wilson-loop approach, Wang et al. [26] demonstrated that the nontrivial winding of the Berry phases can be destroyed by adding trivial bulk bands due to

* Corresponding author.
E-mail address: milan.cajic@swansea.ac.uk (M. Cajić).

https://doi.org/10.1016/j.ijmecsci.2021.106573
Received 5 April 2021; Received in revised form 31 May 2021; Accepted 31 May 2021
Available online 5 June 2021

fragile topology in certain topological classical-wave systems. However, as revealed in [8] for one-dimensional elastic superlattices composed of several masses and spring stiffnesses, a Berry (Zak) phase of individual bands can differ from usual values of 0 or π when the summation of the Berry phases overall bands is an integer multiple of 2π. According to [27], in such cases, the winding number represented by this integer is not an important value in standard discussions of Zak phases which is only meaningful in mod 2π. In our study, this property will be exploited when analysing the topological interface states in an array of coupled beam structures.

One can distinguish two main approaches that are used in mechanical systems to generate interface modes and named upon analog effects in solid physics. The first approach is based on the quantum Hall effect (QHE) that breaks the time-reversal symmetry and belongs to active techniques since it includes components active in time [28]. On the other side, the second approach is passive and it is based on the quantum valley Hall effect (QVHE) or quantum spin Hall effect (QSHE). As given in [29], the coupling of two degenerate wave modes and creation of double Dirac cone along the irreducible Brillouin zone boundary [30] is an important sign of the existence of interface states in mechanical systems. Many studies reported how by breaking the time-reversal symmetry one can generate interface modes [31,32], while Pal et al. [33] investigated the elastic analogs of the quantum valley Hall effect through discrete one and two-dimensional lattices. The aforementioned studies are mostly concerned with linear analysis where interface modes are topologically protected and robust to defects and uncertainties. Recently, Pal et al. [34] investigated the effect of spring nonlinearity on interface modes in discrete one-dimensional spring-mass and two-dimensional lattice systems.

In this study, the main interest is devoted to topological interface modes in one-dimensional elastic phononic crystals. One such system was studied by Yin et al. [35], where topological transition point was confirmed for both longitudinal waves and bending waves. It is worth noting that topological interface states for elastic waves in one-dimensional systems are mostly induced by Bragg scattering. However, Fan et al. [36] demonstrated that it is possible to excite interface state by local resonances in the sub-wavelength range. Similarly, Huang et al. [37] realized topological edge modes in the one-dimensional composite structure as a result of both Bragg scattering and local resonances. Some authors have studied the topologically protected interface modes for both in-plane and out-of-plane [38] bulk elastic waves. Existence of topologically protected interface modes in PCs is a unique property that can be applied to solve many engineering problems in wave localization and isolation [13], control of vibrations, waveguiding [39], acoustic focusing and cloaking [40], energy harvesting [41] etc. In our study, the particular interest is paid to an array of elastic structures that are coupled through elastic medium [42]. For example, Rosa et al. [43] studied the topological pumping in the array of semi-infinite continuous elastic beams coupled through a distributed stiffness showing that adiabatic stiffness modulations along the beams length causes the transition of localized states from one to the opposite boundary of an array. Moreover, some authors raise the question of using the active elastic metamaterials to achieve controllable elastic cloaking [44] or tunable topological states [45].

The majority of studies are limited to the wave propagation analysis of simple sandwich beams with softcore [46] or rigidly connected through periodically distributed ribs [47]. When more complex multiple coupled structures systems are considered, the analyses are mostly limited to dynamic studies of systems with multiple coupled beams [48] or plates [49] through discrete elastic or viscoelastic medium. Recently, Karličić et al. [50] studied the Bloch wave propagation in an array of elastically coupled Rayleigh beams of finite length and with corresponding boundary conditions. Similar configurations of arrays of parallelly connected rods and beams were investigated and exploited in waveguiding applications [39,51,52]. This study is focused on the investigation of topological interface states in such systems and the effect of different parameters on that topology.

Recently, the inerter devices are often used to reduce the vibration responses of various engineering systems [53–55]. As given in [53,56], inerter can be considered as a two-terminal mass element whose terminals can move freely to provide a resisting force proportional to their relative acceleration, where a small actual mass can be magnified into a large apparent mass. Among the first applications of the inerter system are related to the amplification of viscous-damping force [57], while different realizations of these mechanisms are proposed in the literature [58–61]. To model the inerter system, usually the inerter, spring, and damping elements are proposed in the literature based on energy methods [62] or moment of equilibrium equations [63]. Inerters are then used to represent the restoring force in discrete coupled mass-spring systems [64,65], beam structures [66] or nonlinear coupled plates [62,67]. Some recent findings [68] revealed how inertial amplification affects wave dispersion in acoustic metamaterials and demonstrated the possibility to wider the band gaps via inertial amplification. It is well known that active elastic metamaterials have advantages over passive ones since their wave propagation and topological properties can be controlled in real-time without changing their material or geometrical features. On the other side, inerters embedded into the metamaterial or phononic type system are behaving as passive components. However, in [69,70] the authors demonstrated that inerters with easily changeable inertance properties can be constructed and therefore used for tuning of the overall properties of the system.

Inspired by the above studies, we intend to investigate topological interface modes in a multiple beam array system consisting of elastically connected beams of finite length with inerters located in the elastic layers at the interface. In some earlier research papers, the main focus was put on the initial Bloch bands when analysing the interface modes generated in an elastic medium with longitudinal and bending elastic waves [35], with less attention to localization at higher wave modes. Recent investigations included the analysis of multiple interface modes induced by band transitions and exchange in wave mode polarization at both lower and higher wave modes [29]. However, the aforementioned studies are mostly limited to the analysis of one-dimensional phononic type elastic structures observed as beams with periodically varying geometry in the form of changing stepwise circular cross-sections. We aim to show the existence of multiple interface modes in the proposed beam array system at both lower and higher frequency wave modes that are generated by bending vibrations of beams. The corresponding eigenvalue problem will be established and solved to analyse the band structure of the proposed system configuration based on the Euler-Bernoulli beam and Winkler's type elastic foundation models. Band inversion effect with transition points will be demonstrated based on dispersion analysis at the edges of the first Brillouin zone. The existence of interface modes will be illustrated through eigenvalues and frequency response function analysis of a beam array system with a finite number of unit cells. Moreover, the steady-state responses of beams within the beam array system will be studied for different harmonic excitation frequencies to confirm the interface mode localization at the interface. The effect of the so-called defect mass, i.e. the case with some beam in the system having attached concentrated mass, is investigated to demonstrate the robustness of the interface modes to applied changes. The previously mentioned analyses will be repeated for the beam array configuration with inerters at the interface. The influence of the inerter parameter on eigenvalues, frequency response function, and steady-state responses in space will be studied to show its effects on interface modes. This theoretical study will contribute to the understanding of topological mechanics of connected elastic structures and lead to the possible application of passive components such as inerters in the tuning of topologically protected edge modes.

This work is organized as follows: the general mechanical model of the periodic beam array system with elastically coupled beams and

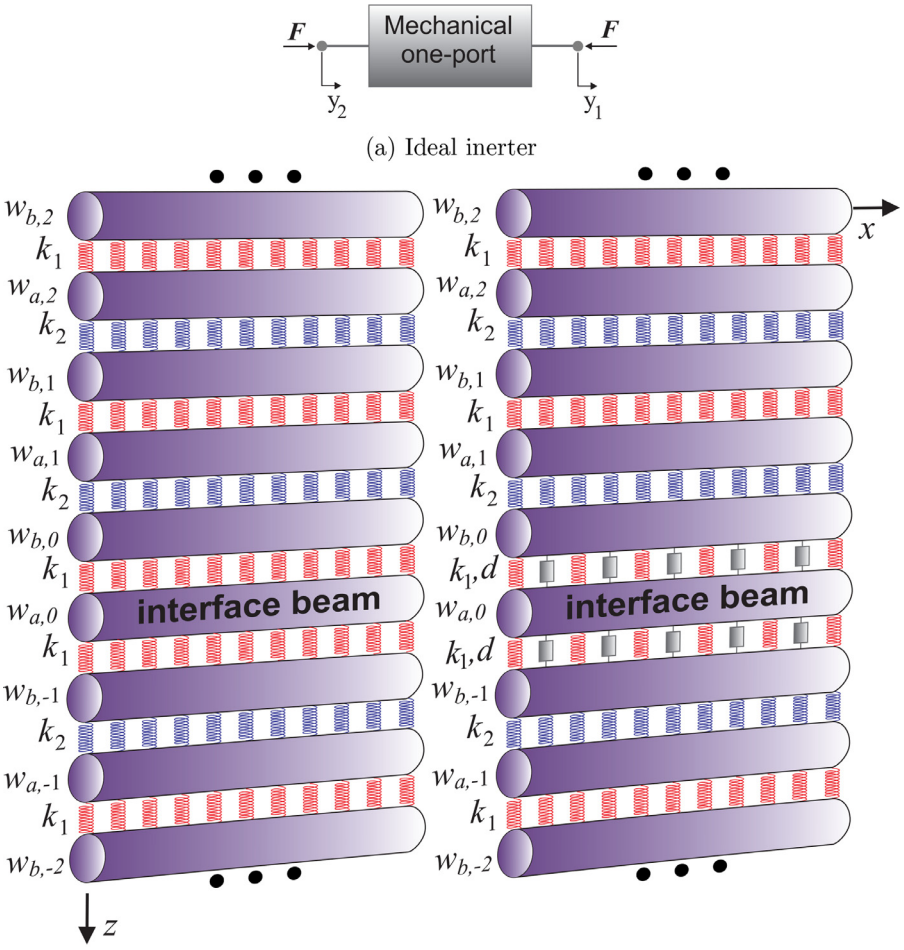

Fig. 1. Illustration of the mechanical inerter and beam array system with two sub-lattices of unit cells which are inverted copies of each other and connected at the interface beam through springs or springs and inerters.

inerters, Galerkin approximation procedure, Floquet-Bloch theorem, the definition of the eigenvalue problem, and derivation of the frequency response function is presented in Section 2. Numerical results for the frequency response function, band inversion, steady-state response in space and particular interface modes of a simple mass-spring-inerter system and chosen configuration of the multiple Euler-Bernoulli beams array systems with and without inerters or defect mass, are given in Section 3. Finally, Section 4 is the conclusion underlying the main contributions and the future work.

2. Problem formulation

2.1. Beam array system with inerters

According to the definition given in [56], the ideal inerter is a mechanical one-port with the property that the equal and opposite forces at the terminals are proportional to the relative acceleration between them. If we consider the two terminals as connection points to other elements (see Fig. 1a for details) and we have displacements y_1 and y_2, we can express the force at the terminal as

$$F(t) = d(\ddot{y}_2(t) - \ddot{y}_1(t))$$

where $d > 0$ is the inertance with units of kilograms. The terminals are also the application points for the forces, which are colinear with the line joining the terminals. Therefore, the main property of the ideal inerter is proportionality between force and relative acceleration.

In this section, an example of a phononic beam array system is given based on the periodically repeating unit cell containing two identical beam elements with the same boundary conditions and coupled through elastic layers of different stiffness properties. It is considered that the beam array system is constructed from two sub-lattices of unit cells that are inverted copies of each other and connected at the interface, where each sub-lattice has n unit cells with two alternating stiffnesses of connecting layers (see Fig. 1b). Unit cells are periodically distributed in z-direction. Ideal inerters are introduced in the coupling layers below and above the interface beam, while other coupling layers remain the same. By introducing the assumptions from the Euler-Bernoulli beam theory and elastic layers with inerters, the governing equation of motion for the interface beam is given as

$$\rho A\ddot{w}_{a,0} + EIw''''_{a,0} + 2d\ddot{w}_{a,0} - d(\ddot{w}_{b,0} + \ddot{w}_{b,-1}) + 2k_1 w_{a,0} - k_1(w_{b,0} + w_{b,-1}) = f_{a,0}(x,t), \quad (1)$$

where $()'''' \equiv \partial^4/\partial x^4, \ddot{()} \equiv \partial^2/\partial t^2$. In general, $w_{u,p}$ and $f_{u,p}(x,t)$ are the displacement and applied periodic force of the u-th beam in the p-th unit cell for $u = a, b$, while ρ, A, E and I denotes beam's density, cross-sectional area, Young's modulus and cross-sectional moment of inertia, respectively. The beams within the unit cell and with neighboring cells are connected through coupling layers of different stiffnesses k_1 and k_2 except at the interface beam, which is from both sides connected with adjacent beams through the coupling layers of the same stiffness k_1 and inertia amplification d properties.

The governing equations for the beams in the unit cells bellow the interface coupled with elastic layers without inerters are given as

$$\rho A\ddot{w}_{a,p} + EIw''''_{a,p} + k_2(w_{a,p} - w_{b,p}) + k_1(w_{a,p} - w_{b,p-1}) = f_{a,p}(x,t), \quad (2)$$

$$\rho A\ddot{w}_{b,p} + EIw''''_{b,p} + k_2(w_{b,p} - w_{a,p}) + k_1(w_{b,p} - w_{a,p+1}) = f_{b,p}(x,t), \quad (3)$$

and for the beams in the unit cells above the interface as

$$\rho A\ddot{w}_{a,p} + EIw''''_{a,p} + k_1(w_{a,p} - w_{b,p}) + k_2(w_{a,p} - w_{b,p-1}) = f_{a,p}(x,t), \quad (4)$$

$$\rho A\ddot{w}_{b,p} + EIw''''_{b,p} + k_1(w_{b,p} - w_{a,p}) + k_2(w_{b,p} - w_{a,p+1}) = f_{b,p}(x,t). \quad (5)$$

For the beam array system with finite number of unit cells, the first and the last equations in the system are different from others if the chain edges are not connected to the fixed base. Moreover, due to the presence of inerters, the equations for the beams bellow and above the interface beam, respectively are given as

$$\rho A\ddot{w}_{b,-1} + EIw''''_{b,-1} + d(\ddot{w}_{b,-1} - \ddot{w}_{a,0}) + k_2(w_{b,-1} - w_{a,-1}) + k_1(w_{b,-1} - w_{a,0}) = f_{b,-1}(x,t), \quad (6)$$

$$\rho A\ddot{w}_{b,0} + EIw''''_{b,0} + d(\ddot{w}_{b,0} - \ddot{w}_{a,0}) + k_1(w_{b,0} - w_{a,0}) + k_2(w_{b,0} - w_{a,1}) = f_{b,0}(x,t). \quad (7)$$

For the beam array configuration presented in Fig. 1b, one can adopt identical boundary conditions on all beams, which for the pinned-pinned (PP) beams are $w_{u,p}(0,t) = w''_{u,p}(0,t) = w_{u,p}(L,t) = w''_{u,p}(L,t) = 0$, $u = a, b$. Similar to this, one can easily adopt other types of boundary conditions such as clamped-clamped (CC) beam configuration, which would require only changes in the adopted mode shape functions in the Galerkin approximation to calculate frequency responses and band structure of the system.

In the case when one of the beams is having Ξ attached concentrated masses, the overall mass of that beam is changed and it can be considered as a defect mass in the chain. This yields a different governing equation, which for some beam in the p-th unit cell below the interface is given as

$$(\rho A + \sum_{\xi=1}^{\Xi} m_\xi \delta(x - \sigma_\xi))\ddot{w}_{a,p} + EIw''''_{a,p} + k_2(w_{a,p} - w_{b,p}) + k_1(w_{a,p} - w_{b,p-1}) = f_{a,p}(x,t), \quad (8)$$

or

$$(\rho A + \sum_{\xi=1}^{\Xi} m_\xi \delta(x - \sigma_\xi))\ddot{w}_{b,p} + EIw''''_{b,p} + k_2(w_{b,p} - w_{a,p}) + k_1(w_{b,p} - w_{a,p+1}) = f_{b,p}(x,t), \quad (9)$$

where σ_ξ is the position of ξ-th mass on the beam and δ is the Dirac function.

2.2. The eigenvalue problem and frequency response function

The first step is to discretize the motion equations of the unit cell by using the Galerkin approximation. The solution is assumed in the following form

$$w_{u,p}(x,t) = \sum_{r=1}^{N} q_{(u,p)r}(t)\phi_{(u,p)r}(x), \quad u = a, b, \quad (10)$$

where $q_{(u,p)r}$ and $\phi_{(u,p)r}$ are the generalized time functions and assumed trial (mode shape) functions of the bare beam, respectively. N is the number of adopted terms in the Galerkin approximation series. In structural dynamic problems, the mode shape functions satisfying the boundary conditions are often used in the method of separation of variables to solve the PDEs. If the beam array configuration without concentrated masses is observed, applied mode shape functions of the bare beam also satisfy the boundary conditions and the obtained solution can be considered as the exact one for the finite number of adopted modes. The application of the Galerkin approximation comes into the effect when the case with concentrated masses is observed, where the adopted mode shape functions of the bare beam are not the exact functions satisfying the boundary conditions. In that case, the accuracy of the obtained approximated solution can be increased by adopting the higher number of terms in the Galerkin approximation.

Inserting Eq. (10) into the governing Eqs. (1)-(9), multiplying them with the corresponding trial functions, integrating over the beam's domain and taking into account corresponding orthogonality conditions (see Appendix A) gives matrix equations of the form

$$\mathbf{M}\ddot{\mathbf{q}} + \mathbf{K}\mathbf{q} = \mathbf{f}, \quad (11)$$

where $\mathbf{M}$ is the mass matrix and $\mathbf{K}$ is the stiffness matrix of the system, while $\mathbf{f}$ is the force vector. By introducing the harmonic solution of the form $\mathbf{q} = \overline{\mathbf{q}}e^{j\omega t}$, $j = \sqrt{-1}$, and taking that $\mathbf{f} = 0$, yields the following eigenvalue problem

$$(\mathbf{K} - \omega^2\mathbf{M})\overline{\mathbf{q}} = 0. \quad (12)$$

The elements of the stiffness $\mathbf{K}$ and mass matrix $\mathbf{M}$ are given in the Appendix A. By solving the above eigenvalue problem for a finite number of unit cells and adopted terms in the Galerkin approximation, one can detect interface modes which are located within the band gaps. To confirm the existence of localized modes, we will determine the frequency response function of the system by assuming the harmonic force $F_0e^{j\Omega}$ acting on the last beam $w_{(b,-n)}$ bellow the interface such that $\tilde{f}_{(b,-n)k} = F_0e^{j\hat{\Omega}}\int_0^L \delta(x-\zeta)\phi_{(b,-n)k}(x)dx = F_0e^{j\hat{\Omega}}\phi_{(b,-n)k}(\zeta)$.

2.3. Band inversion

Let us assume that the infinite beam array system is composed of unit cells with two identical beams coupled mutually and with adjacent unit cells through springs of different stiffnesses $k_1 = k(1+\gamma)$ and $k_2 = k(1-\gamma)$. If we chose some p-th unit cell described via equation of the form as Eqs. (4) and (5) when $f_{(a,p)} = 0$ and $f_{(b,p)} = 0$. The unit cells can be identified by considering the following notation $p + v$, with $v = -1, 0, 1$ denoting the previous, present, and subsequent unit cell, respectively. Then, by taking the above Galerkin approximation and the Floquet-Bloch theorem for the plane wave solution of the form

$$q_{(u,p+v)r} = Q_{(u)r}(\mu)e^{j(\omega t + \mu a(p+v))}, \quad u = a, b, \quad (13)$$

one can obtain the matrix equation as

$$(\mathbf{K}_p - \omega^2\mathbf{M}_p)\tilde{\mathbf{q}} = \left(\begin{bmatrix} \mathbf{K}_{11}^{a,p} & \mathbf{K}_{12}^{a,p}(\mu) \\ \mathbf{K}_{21}^{b,p}(\mu) & \mathbf{K}_{22}^{b,p} \end{bmatrix} - \omega^2 \begin{bmatrix} \mathbf{M}_1^{a,p} & \mathbf{0} \\ \mathbf{0} & \mathbf{M}_2^{b,p} \end{bmatrix}\right)\begin{bmatrix} \mathbf{q}_1^{a,p} \\ \mathbf{q}_2^{b,p} \end{bmatrix} = 0, \quad (14)$$

where $\tilde{\mathbf{q}}$ is the vector of wave amplitudes while elements of matrices $\mathbf{K}_p$ and $\mathbf{M}_p$ of dimension $2N \times 2N$ are given in Appendix B. By solving this inverse eigenvalue problem in Eq. (14) one can obtain m eigenvalues ω_m and eigenvectors $\tilde{\mathbf{q}}_m$ as functions of the wave propagation constant μ, which will yield corresponding dispersion relations. Moreover, by investigating the eigenvectors of the beam array system one can additionally examine topological features of eigensolutions when stiffness parameter γ is varied as a positive and negative value. This kind of analysis can provide us with information on the existence of band inversion in the beam array system. As explained in [34], in a one-dimensional mass-spring lattice system one can observe a change of eigenvectors for varying wavenumber μ over the first Brillouin zone. According to this, the transformation of stiffness parameter γ from positive to negative values can change the eigenvectors but not eigenvalues. The same transformation can be achieved by reversing the direction of the lattice basis vector or through the translation of the unit cell by one mass in the chain. These transformations are attributed to changes in the gauge, which then changes the eigenvectors and the topology of the vector bundle related to the solution of the corresponding eigenvalue problem. The topology of this vector bundle can be evaluated by using the Zak phase

for the bands, which is a special case of the Berry phase used to characterize the band topology and band inversion in 1D periodic media. For some m-th band, the Zak phase can be calculated as

$$Z = \int_{-\pi}^{\pi} \left[j(\tilde{\mathbf{q}}_m(\mu))^H \cdot \partial_\mu \tilde{\mathbf{q}}_m(\mu) \right] d\mu \tag{15}$$

where $(\tilde{\mathbf{q}}_m(\mu))^H$ is the Hermitian of eigenvector $\tilde{\mathbf{q}}_m(\mu)$. A more simplified discretized form of Eq. (15) can be used in numerical calculation of the Zak phase as

$$\Theta^{Zak} = -\mathrm{Im} \sum_{c=-P}^{P-1} \ln\left[\tilde{\mathbf{q}}_m^H\left(\frac{c}{P}\pi\right) \cdot \tilde{\mathbf{q}}_m\left(\frac{c+1}{P}\pi\right) \right] \tag{16}$$

The Zak phase need to be calculated for each band and it usually take values $\Theta^{Zak} = 0$ and $\Theta^{Zak} = \pi$. Since the Zak phase is not gauge invariant, the choice of coordinate reference and a unit cell must remain the same during computation. Therefore, the Zak phase can give us important information about the geometric phases of the bulk band and the existence of interface modes in different PC configurations [29]. However, despite the fact that from Eq. (14) one can easily determine the resulting eigenvalues and eigenvectors, above Eqs. (15) and (16) seem to be inapplicable to the present problem since aforementioned values of the Zak phase $\Theta^{Zak} = 0$ or $\Theta^{Zak} = \pi$ cannot be obtained for individual bands. This will be elaborated additionally in the following section.

One can also predict the generation of interface modes when there is a mode transition frequency (band transition point) between the band gaps of topologically distinct PCs. More precisely, interface modes can be induced by varying the symmetry of the band-edge states at both the upper and lower edges of the band gap. It should be noted that for the beam array system with inerters at the interface, the dispersion relations cannot be constructed via the classical Floquet-Bloch approach since it requires that all unit cells in the system are identical. Either way, in the following numerical analysis the bulk band of a beam array system with inerters will be computed to reveal the effect of inerters on band inversion. This requires only minor changes in the mass matrix from Eq. (14) to account for the effect of inerters in the representative unit cell.

3. Numerical results

In this section, the results for the frequency response function (FRF) and band structure will be given first to demonstrate the existence of interface modes in the coupled multiple beam array system without inerters. Further, the influence of inerters in discrete mass-spring and multiple beam array systems will be investigated to reveal their effect on interface modes. The following values of parameters are adopted in numerical simulations if not given differently: Young's modulus $E = 3.2 \cdot 10^9$[Pa], cross-sectional moment of area $I = 4.5 \cdot 10^{-11}$[m^4], beams length $L = 0.8$[m], cross-sectional area $A = 6 \cdot 10^{-5}$, density $\rho = 1190$[kg/m^3], and mean stiffness $k = 200$[N/m^2] related to stiffnesses $k_1 = k(1+\gamma)$ and $k_2 = k(1-\gamma)$, with γ denoting the dimensionless stiffness parameter. All given numerical examples of a beam array system without defect mass are calculated for adopted $N = 5$ terms in the Galerkin approximation, which enables us to study all the important interface modes in the lower and higher frequency range. For the reasons mentioned previously, the number of adopted terms in the Galerkin approximation is increased to $N = 10$ for the configuration where the so-called defect mass is introduced. When calculating the FRF, a beam array system with a finite number of $n = 10$ units cells on each side of the interface is considered, where beams at the two opposite ends of the chain are free (not connected to the fixed base) and denoted as $w_{b,-10}$ and $w_{b,10}$. The whole system is having an odd number of beams such that the beam denoted as $w_{b,0}$ is in the center. Here, we will consider as symmetric those modes where displacement of the interface beam is equal to zero while adjacent beams are oscillating with the same amplitude but opposite phase. This is not the case with the anti-symmetric modes, where beams adjacent to the interface are in phase and the interface displacement is different from zero. Therefore, we measure the frequency response of the beam $w_{b,0}$ presuming that displacement of the interface beam displacement $w_{a,0}$ in symmetric modes is equal to zero. It should be noted that in the FRF analysis, the harmonic force is acting on the last beam $w_{b,-10}$ at the point $\zeta = 0.45L[m]$, to move it away from the central node (point with zero displacements in certain mode shapes of the pinned-pinned beam). Steady-state responses are calculated based on a methodology similar to those found in [71], where convolution integral solution is applied to determine the steady-state amplitudes. All the responses are measured at the point $x = 0.55L$.

3.1. Beam array system without inerters

First, we will show the example of a finite beam array system without inerters. This includes both, showing the eigenvalue analysis and frequency response function that are plotted for frequencies normalized with the first natural frequency of the simply supported bare beam. Figure 2 shows eigenvalues (left) and FRF (right) of the beam array system with an interface for adopted five modes in the Galerkin approximation. It illustrates several narrow passbands and band gaps as well as interface modes at both lower and higher frequency ranges for the value of stiffness parameter $\gamma = 0.5$ ($k_1 > k_2$), where interface modes are localized within the narrow band gaps, see Fig. 2a. Figure 2b shows eigenvalues and FRF of the beam array system when $\gamma = -0.5$ is a negative value, i.e. in the case where the stiffness of layers below and above the interface beam is weak ($k_1 < k_2$). Here, the majority of interface modes migrate into the bulk indicating their trivial nature but certain interface modes remain inside the band gaps. A similar effect can be viewed in 1D phononic mass-spring chains [33], when the unit cell configuration includes two identical masses and two springs of different stiffness properties. In our case, one can notice the existence of multiple bands and higher frequency interface modes since instead of discrete mass-springs, continuous beam structures are used. It is well known that continuous structures are having an infinite number of degrees of freedom and mode shapes. However, we depicted only the lower modes which can be encompassed by the five-term Galerkin approximation. It is interesting to note that in all four sub-figures one can identify a band gap that starts from a zero frequency, with no interface modes detected inside it. Such obtained band gap is a specific feature of the proposed beam array system that was found earlier in [50] and explained with more details.

Normalized steady-state displacement amplitudes (red asterisks) are given in Fig. 3 to demonstrate the existence of interface modes in space. Normalization in this case is performed by dividing all amplitudes with the maximal steady-state amplitude for the current beam array configuration. Here, the beam array system with $n = 15$ unit cell on each side of the interface and sixty one beams in the system is considered, where harmonic excitation is applied to the first beam below the interface denoted as $w_{b,-15}$. The beam array configuration with adjacent high stiffness springs $\gamma = 0.5$ at the interface is considered as an example. Four different interface modes are presented for the cases when the harmonic excitation is near the resonant (interface) frequency. Modes are counted as they appear in Fig. 2a, starting from the lowest frequency interface mode. It should be noted that frequencies given in figures are truncated to four decimal places for convenience but the exact values should be calculated for the repetition of the results. It can be noticed that all given interface modes except one can be characterized as symmetric since the interface beam is at rest while the neighboring beams are oscillating with the same amplitude (but opposite phase). The third given interface mode (upper right sub-figure) can be considered as the anti-symmetric one since the amplitudes of the interface and adjacent beams are different from zero (they are oscillating in phase).

Fig. 4 shows dispersion curves and band inversion in the beam array system at the limits $\mu = \pi$ of the first Brillouin zone, which is obtained by solving the eigenvalue problem from Eq. (14). Fig. 4a and c shows several branches and band gaps at lower and higher frequency ranges for

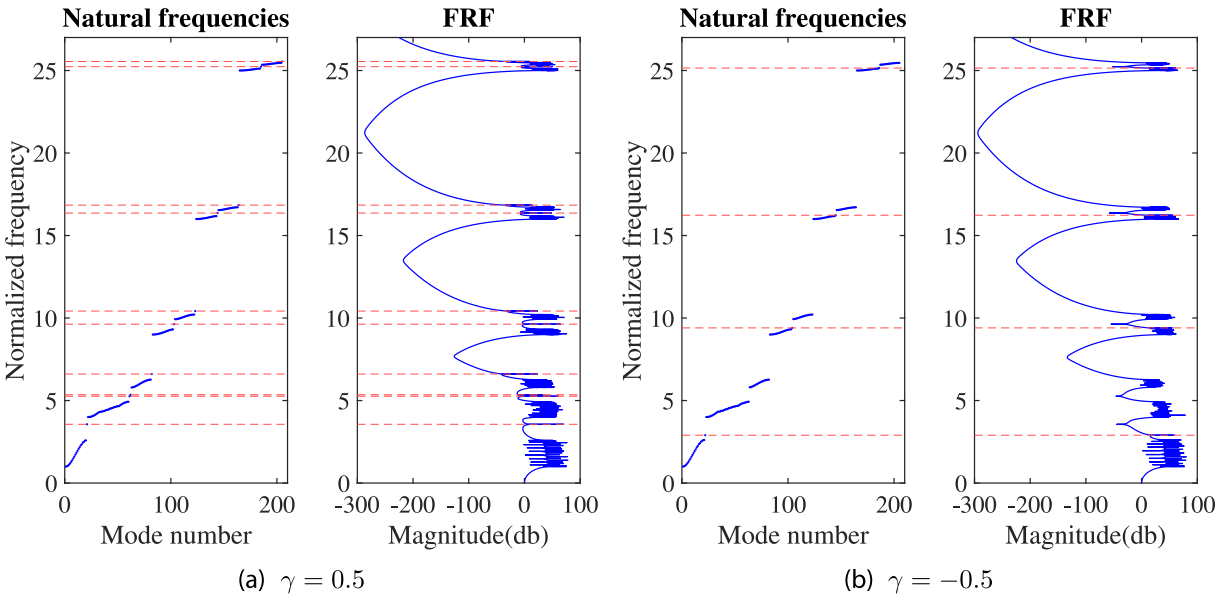

Fig. 2. Natural frequencies and frequency response function of the elastically coupled beam array system given in two different configurations $k_1 < k_2$ and $k_1 > k_2$.

the value of stiffness parameter $\gamma = 0.5$ and $\gamma = -0.5$, respectively. It can be noticed that the band structure does not change under transformation $\gamma \to -\gamma$, which means that eigenvalues are not changing, which is not the case with eigenvectors. Narrow band gaps existing between some branches are vanishing for $\gamma = 0$ (the case with all identical springs), where band gaps are closing at the edges of the first Brillouin zone. As revealed in [72] for diatomic lattices, the transition between acoustic and optical frequencies from approaching to veering, a phenomenon called eigenvalue loci veering (avoided-crossing), occurs when the band gap is closing i.e. it requires non-trivial topology. In other words, veering is a consequence of rapid variation in the eigenvectors, which can then cause band inversion or band localization. Similar behavior can be noticed in our case but for several bands at lower as well as higher frequency ranges. Whether certain edge (interface) modes are trivial or not can be illustrated by calculating the invariants associated with separate bands i.e. the topology of their vector bundles, which is usually characterized through the Zak phase. However, as stated earlier in the text, calculating the Zak phase of individual bands in a multi-band system can be a difficult task. In our case, when using the Eq. (16) to calculate the Zak phase for ten bands obtained from the eigenvalue problem in Eq. (14) yields values of Zak phases which are different from the usual 0 or π but whose summation yields the integer multiple of 2π. As given by [27], such obtained value is not important from the perspective of standard discussion of the Zak phase and will not be elaborated further in this study. Fig. 4d demonstrates the existence of band inversion when γ is varied from minus to plus values. Moreover, one can easily notice multiple band inversions at both, lower and higher frequencies, thus indicating the existence of localized modes.

3.2. The effect of defect mass

As given by Eqs. (8) and (9), the concentrated mass attached to the random beam in the system changes the mass matrix of the system. The beam with changed mass compared to other beams in the system can be considered as a defect mass in the chain. Here, we investigate whether this defect may cause changes in the interface modes of the adopted beam array configuration. It is well known that the main property of the topologically protected interface modes is their robustness to defects and disorders. Defect mass is represented by the single concentrated mass $m_1 = m\rho AL$ attached at the mid-span $\sigma_1 = 0.5L$ of the beam denoted as $w_{a,-10}$. For this purpose, a case with $n = 20$ unit cells on each side of the interface is adopted as well as $N = 10$ terms in the Galerkin approximation.

In Fig. 5 we depicted four different cases of the value of concentrated mass attached at the beam denoted as $w_{a,-10}$. One can observe that all of the interface modes (red dashed lines) that exist in the system without defect mass remain the same in the system with the defect mass. However, some new defect modes emerge inside the frequency band gaps by gradually increasing the value of the attached mass (see black dash-dotted lines in Fig. 5). More precisely, only two additional defect modes emerge in higher frequency band gaps for the lower values of mass (second sub-figure from the left side) while four and five additional defect modes are present in both lower and higher frequency band gaps for the higher values of attached mass (third and fourth sub-figure from the left side). The obtained frequencies of the defect modes mismatch with the frequencies of the interface modes and are localized in the chain at the place of the defect mass i.e. in the beam with attached concentrated mass denoted as $w_{a,-10}$. Interface modes of the beam array system without and with the defect mass remain the same in all four configurations and are not affected by changes and different mass distribution in the system. Therefore, interface modes are immune to the presence of defect mass in the system. Moreover, an increase in the number of terms in the Galerkin approximation also does not affect interface modes due to previously mentioned reasons. It should be noted that the numbers of unit cells and terms in the Galerkin approximation are increased mostly to contribute to more precise determination of newly emerged defect modes. Since these modes are affected by changes of the mass, the case with $N = 10$ terms in the Galerkin approximation is used to achieve higher accuracy.

3.3. Mass-spring-inerter system

For the sake of simplicity and more clear insight into the effect of inerters on interface modes, we first show the frequency response function of the discrete mass-spring-inerter chain system with the interface, which is composed of unit cells with two identical masses having displacements denoted as $y_{(a,p)}$ and $y_{(b,p)}$, with p denoting the unit cell number. The corresponding equations are derived in Appendix C. Masses and unit cells are mutually connected through springs with stiffness properties $k_1^s = \kappa(1+\gamma)$, $k_2^s = \kappa(1-\gamma)$ with κ being the mean stiffness and γ denoting the dimensionless stiffness parameter. Parameters are nondimensionalized (see Appendix C) such that stiffness related parameters

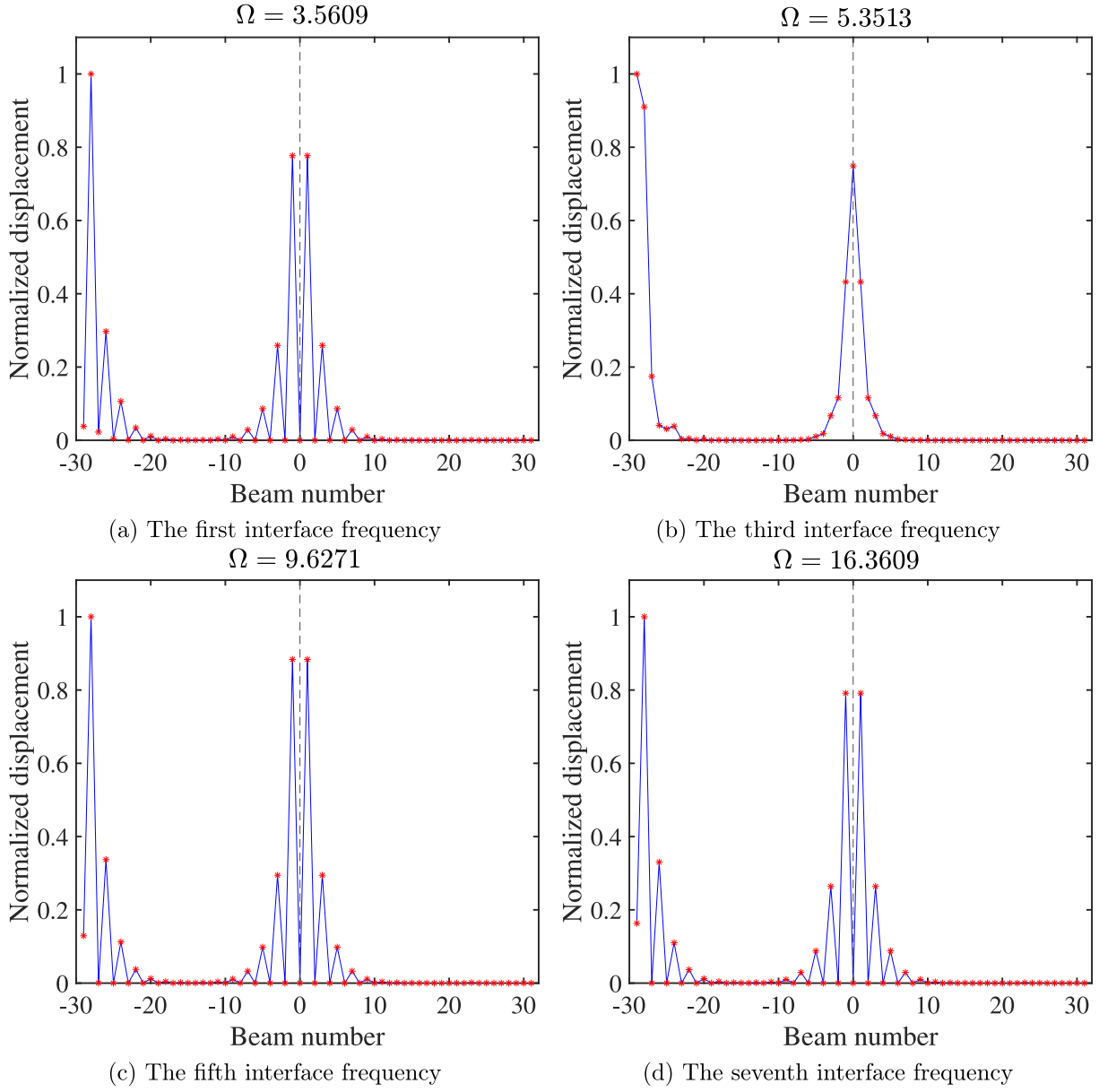

Fig. 3. Normalized steady-state displacement amplitudes of the beam array system with $n = 15$ unit cells on each side of the interface and the first beam $w_{b,-15}$ excited near the interface frequency.

become $\tilde{k}_1^s = 1 + \gamma$ and $\tilde{k}_2^s = 1 - \gamma$ while inertance is characterized by the dimensionless inertia parameter denoted as $\tilde{d}$. The case of the mass-spring-inerter chain with $n = 30$ unit cells on each side of the interface is adopted, with the interface mass denoted as $y_{(a,0)}$ and end masses given as $y_{(b,-30)}$ and $y_{(b,30)}$. The value of dimensionless stiffness parameter $\gamma = 0.4$ is adopted in both cases. We assume that the left end of the chain is fixed and the other is free, and we compute the frequency response function assuming that $y_{(b,-30)} = F_0 e^{i\Omega t}$, $F_0 = 1$ for the mass at the left boundary. Fig. 6 shows the case when $\tilde{d} = 0$, i.e. when the pure mass-spring chain is considered, while the second case belongs to the mass-spring-inerter chain system with the value of inerter parameter $\tilde{d} = 0.1$. FRF is measured for the central mass $y_{(b,0)}$ in the chain (not the interface mass $y_{(a,0)}$). In the pure mass-spring chain one can observe interface modes at the frequency $\Omega = \sqrt{2}$ for symmetric and $\Omega > 2$ for the anti-symmetric mode as revealed in [34], Fig. 6a. By introducing the inerter, one can notice an obvious shifting of interface mode frequencies towards lower values for both symmetric and anti-symmetric modes. However, this shifting is more pronounced at the higher frequency interface mode than for the lower one located inside the band gap.

The effect of inerters on interface modes in the mass-spring-inerter system can be seen more clearly in Fig. 7. The eigenvalues are calculated for the mass-spring and mass-spring-inerter system with $n = 30$ unit cells on each side of the interface. Corresponding interface mode frequencies from Fig. 6 are detected and plotted for varying stiffness parameter γ. The first, lower frequency interface mode, is given in Fig. 7a for the pure mass-spring and two different cases of the mass-spring-inerter system. The second, higher frequency interface mode, is given in Fig. 7b for the same values of parameters. In the case of the pure mass-spring system ($\tilde{d} = 0$) and the first interface mode one can notice that the frequency is changing for $\gamma < 0$ while it is constant for $\gamma > 0$. As explained in [34], this behavior is attributed to the property of symmetric modes that changing the stiffness of springs on both sides of the interface does not change the dynamics of the interface mass. Also, this interface mode is considered to be symmetric only for $\gamma > 0$ and it is independent of γ. In the

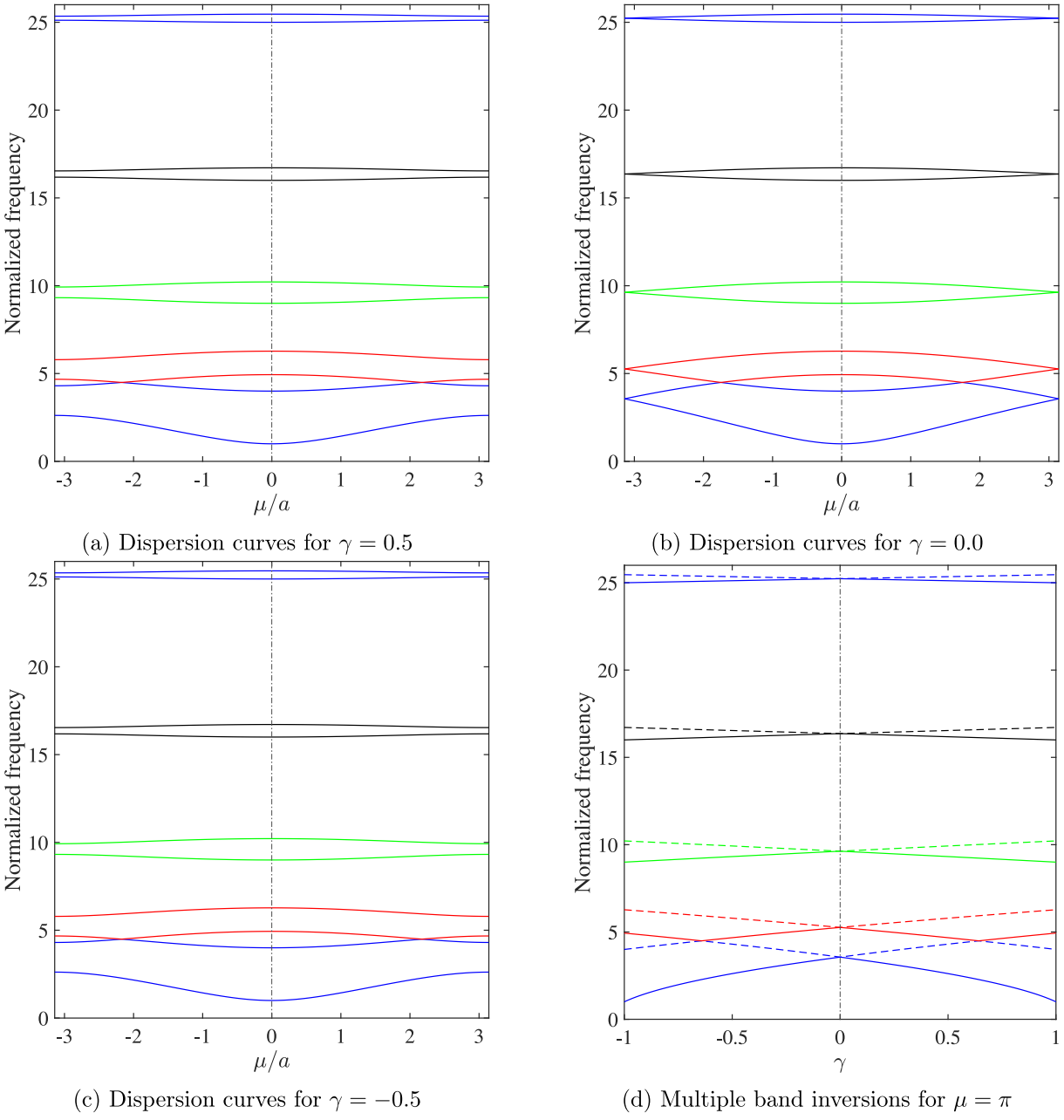

(a) Dispersion curves for $\gamma = 0.5$

(b) Dispersion curves for $\gamma = 0.0$

(c) Dispersion curves for $\gamma = -0.5$

(d) Multiple band inversions for $\mu = \pi$

Fig. 4. Dispersion curves and band inversion of the elastically coupled beam array system without inerters.

case of the second interface mode (Fig. 7b), which is considered to be anti-symmetric and trivial defect mode (it vanish for $\gamma < 0$), it emerges from the bulk, and its frequency increases for positive and increasing value of stiffness parameter γ. The main effect of the inerter parameter that can be observed from this analysis reflects in a decrease of the frequency of interface modes in both, varying and the constant part of the line. Therefore, in the mass-spring-inerter system, the interface mode frequency can be shifted towards lower frequencies by varying the inerter parameter while preserving the main properties and nature of these modes.

3.4. Beam array system with inerters

Fig. 8 displays band inversion of the elastic beam array system for the representative unit cell with inerters. The results are given for the limits of the band gap ($\mu = \pi$) and variations of the parameter γ. By computing the bulk band of a beam array system with inerters, we can additionally investigate the effect of inerters on band inversion. If we compare band inversion plots of the beam array system in two different cases, with lower $d = 0.0001$ and higher $d = 0.001$ values of the inerter parameter, one can notice an obvious shifting of band inversion points towards positive values of γ and lower frequencies. The shift of the degeneracy point is more clear at higher frequencies. More precisely, band inversion points in a beam array without inerters are all located at $\gamma = 0$ (Fig. 4d) while by introducing the inerters one can notice that the bulk band degeneracies shift towards positive values of γ with decreasing frequency, even for small values of the inerter parameter d. The obtained results indicate that the system is very sensitive to changes of the inerter parameter, and therefore interface states will be significantly distinct from those of the system without them, especially for higher frequency interface modes.

Similar to the discrete mass-spring-inerter chain, we can now study the interface modes in the beam array system with inerters at the in-

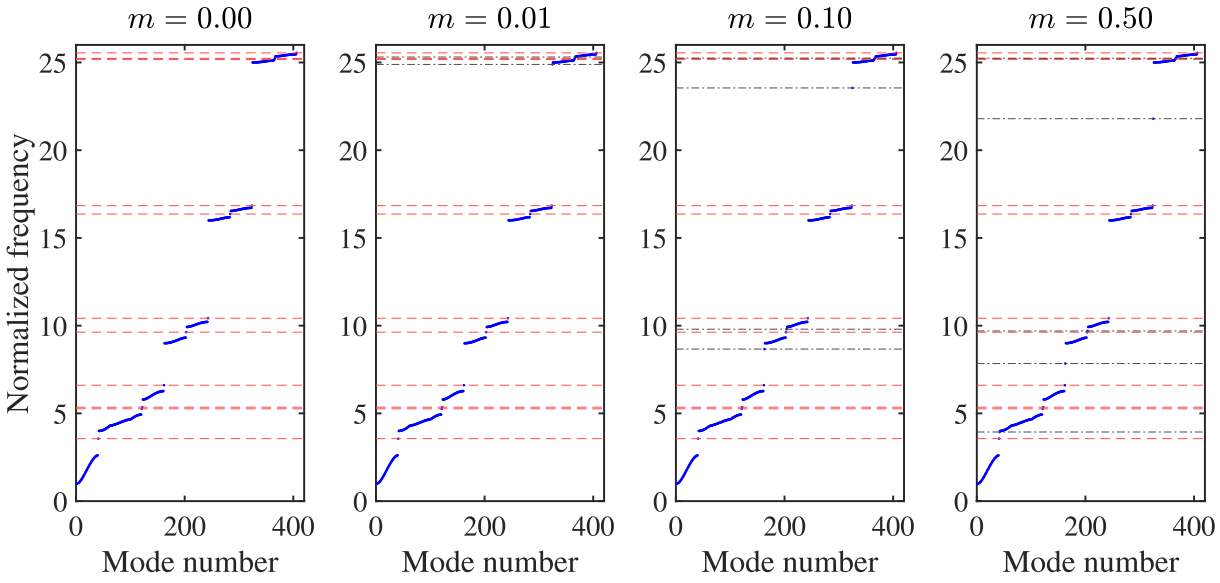

Fig. 5. Interface (red dashed lines) and defect (black dash-dotted lines) modes of the beam array system with and without defect mass for $n = 20$ unit cells on each side of the interface and $N = 10$ terms in the Galerkin approximation.

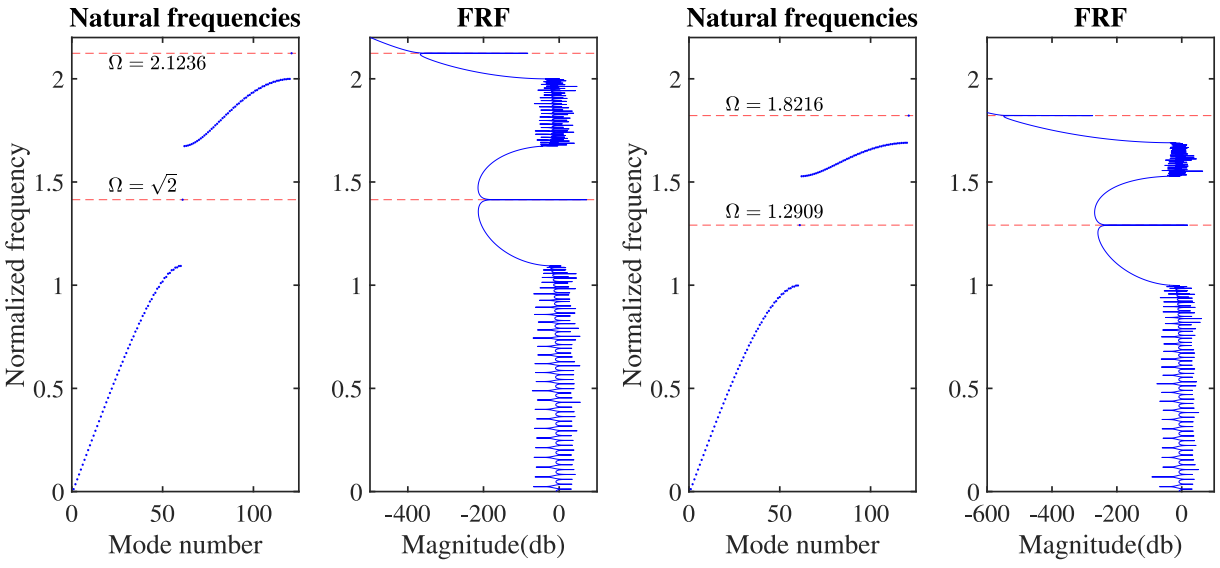

Fig. 6. Natural frequencies and frequency response function of the mass-spring and mass-spring-inerter system for $\gamma = 0.4$ and $n = 30$ unit cells on each side of the interface.

terface (see Fig. 1b). To investigate this, we show the eigenvalues and FRF of the proposed configuration for the value of dimensionless stiffness parameter $\gamma = 0.5$ and two different values of inerter parameter $d = 0.001$ and $d = 0.01$, Fig. 9. It demonstrates the existence of interface modes in both lower and higher frequency band gaps. By introducing and increasing the inertia parameter, one can notice a slight shifting of existing interface modes towards lower frequencies. However, when speaking about lower frequency interface modes, one can notice that they remain within the same band gaps while those at higher frequencies migrate into the bulk or towards lower frequency band gaps. More precisely, in the configuration without inerters (Fig. 2) the higher frequency interface modes are located within the narrow band gaps while in the inerter case they appear in the wide band gaps below them.

Here, similar to the trivial case in Fig. 2b, we intend to investigate the behavior of interface modes of the beam array with inerters in the configuration $\gamma = -0.5$ i.e. when $k_1 < k_2$. Fig. 10 shows FRF of the beam array system for two different values of the inerter parameter $d = 0.001$ and $d = 0.01$. One can notice only fewer interface modes in the configuration without inerters (Fig. 2b) or even fewer number of them in the configuration with inerters but with a low value of inerter parameter $d = 0.001$, see Fig. 10a. This means that the remaining modes migrate into the bulk due to the decreased frequencies caused by the presence of inerters at the interface. By increasing the inerter parameter in Fig. 10b, one can observe the emergence of several interface modes localized in the higher frequency band gaps. This agrees well with the previous findings for the bulk band that the presence of inerters mostly affects higher frequency bands. Even though the nature of the effect of the inerter on higher frequency interface modes cannot be clearly explained, it is obvious that it only slightly changes the lower frequency interface modes.

To demonstrate the interface modes in space for the beam array system with inerters, normalized steady-state displacements are plotted in Figs. 11 and 12 for two different values of inerter parameter. In both

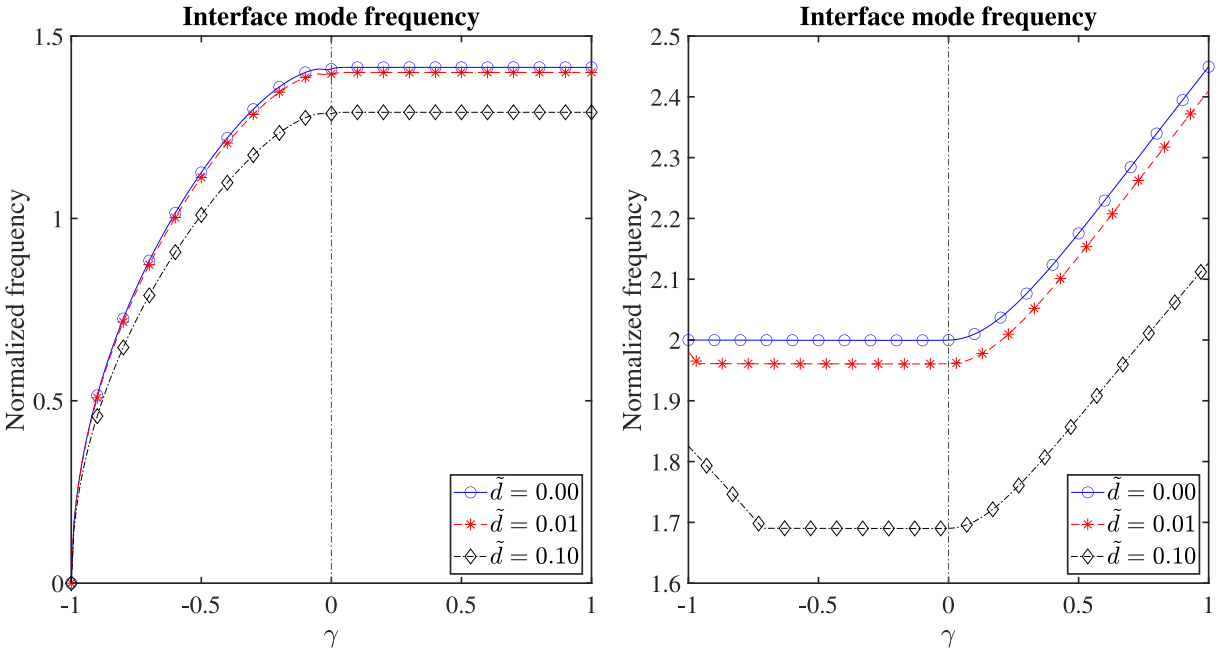

Fig. 7. Interface mode frequencies of the mass-spring and mass-spring-inerter system for varying γ and and different values of dimensionless inerter parameter $\tilde{d}$.

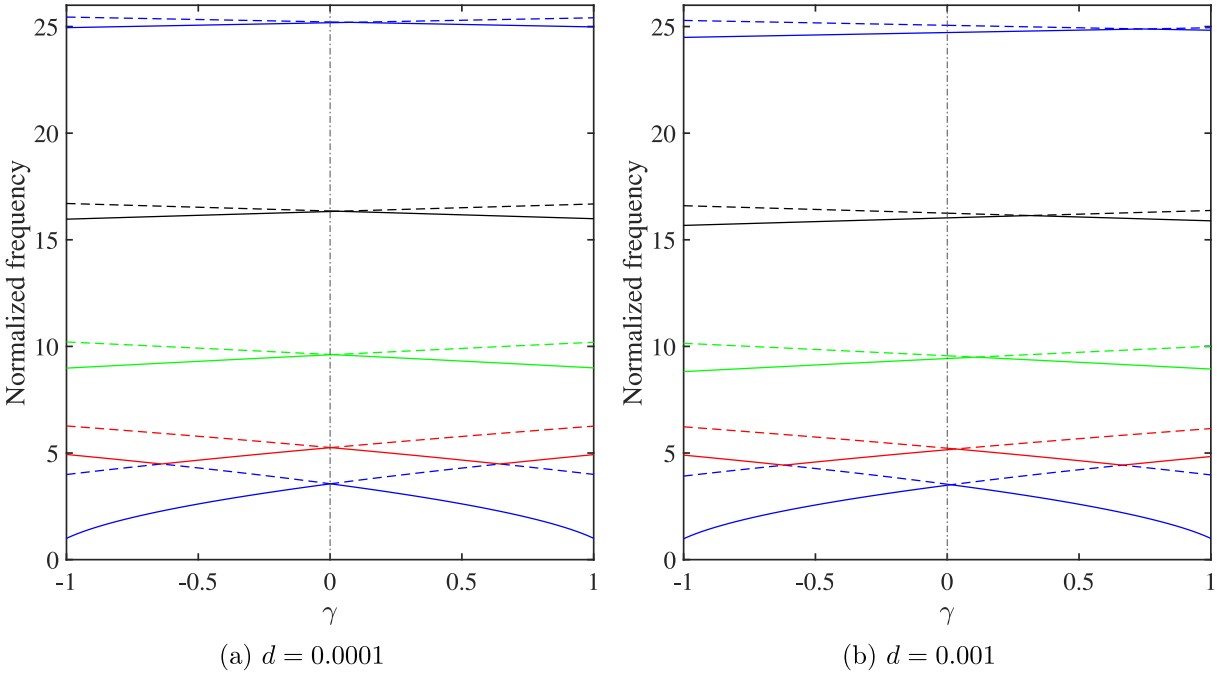

Fig. 8. Band inversion of the elastically coupled beam array system with inerters and different values of the inerter parameter d.

cases, only the first and the third interface frequencies (see Fig. 9 for details) is given when the harmonic excitation is near the resonant frequency. It can be noticed that the first interface mode is the symmetric one since the interface beam is at rest while the adjacent ones oscillate with the same amplitude (but opposite phase). On the other side, the third interface mode is the anti-symmetric one since the amplitudes of the interface and adjacent beams are different from zero (they are oscillating in phase). It should be noted that the discrepancy between the second and third modes in Fig. 9a is very small and can be viewed only by zooming that particular frequency range. However, based on presented results one can notice that the first interface mode given in Fig. 12a appears at a lower frequency for an increase of the value of the inerter parameter. On the other side, the third interface mode (see Fig. 9b) given in Fig. 12b occurs at a higher frequency. This interface mode is newly emerged and it does not correspond to the third mode from Figs. 9a and 11b, since that mode now becomes the second one and it almost migrates into the bulk (see Fig. 9b for details). This can be checked by gradually increasing the value of the inerter parameter.

Finally, to show the tuning potential of the inerter on interface modes in the beam array system, we investigate the behavior of particular in-

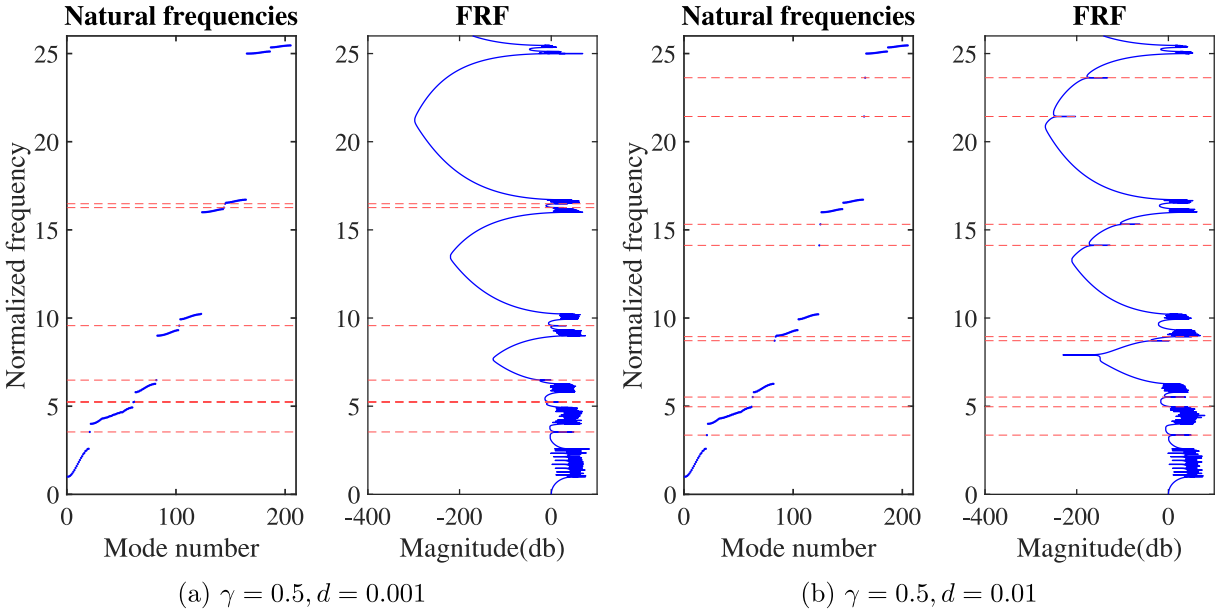

Fig. 9. Natural frequencies and frequency response function of the elastically coupled beam array system with inerters and given in the configuration $k_1 > k_2$.

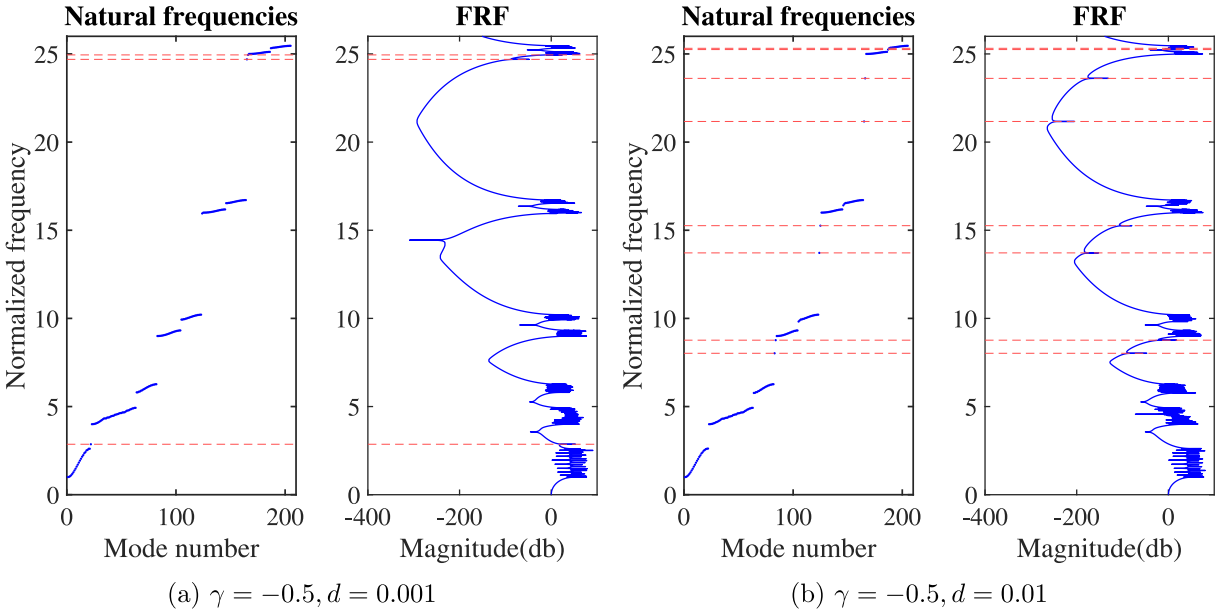

Fig. 10. Natural frequencies and frequency response function of the elastically coupled beam array system with inerters and given in the configuration $k_1 < k_2$.

terface modes for varying stiffness parameter γ and for three different values of the inerter parameter. In that regard, we chose two interface modes from Fig. 2a, the first at the lowest frequency (the first red dashed line) and the next one at the higher frequency (the fifth red dashed line). Fig. 13a shows the lower frequency interface mode for varying stiffness parameter γ and three different values of the inerter parameter d. One can notice that for the case without inerter $d = 0$, the interface mode frequency is increasing while γ is negative, which then becomes constant for positive values of γ. Similar behavior can be noticed in Fig. 13b for the higher frequency interface mode when $d = 0$. This behavior at certain interface modes is similar to the behavior of symmetric interface modes in the simple mass-spring model given in Fig. 7a. By introducing the inerters, this behavior is affected and the frequency starts to decrease for $\gamma > 0$. This effect is even more pronounced in the higher frequency interface mode in Fig. 13b. However, this is different from the results obtained for the mass-spring-inerter system, where the frequency of the interface mode decreases for both $\gamma > 0$ and $\gamma < 0$ while the symmetry properties are preserved. In the case of a beam array system with inerters, the frequencies of interface modes decrease due to the mass amplification effect of inerters. However, one can notice that observed interface modes are independent of the inerter parameter when $\gamma < 0$, which can be attributed to the fact that inerters are introduced only at the interface and the weak interface coupling ($k_1 < k_2$) localized modes are not affected by changes of the inertance.

4. Conclusion

This work demonstrates how localized modes can be induced at the interface of a one-dimensional beam array system with beams mutually connected through elastic layers with two alternating stiffnesses. Governing equations are discretized and matrices for the corresponding eigenvalue problem obtained to calculate the eigenvalues, frequency re-

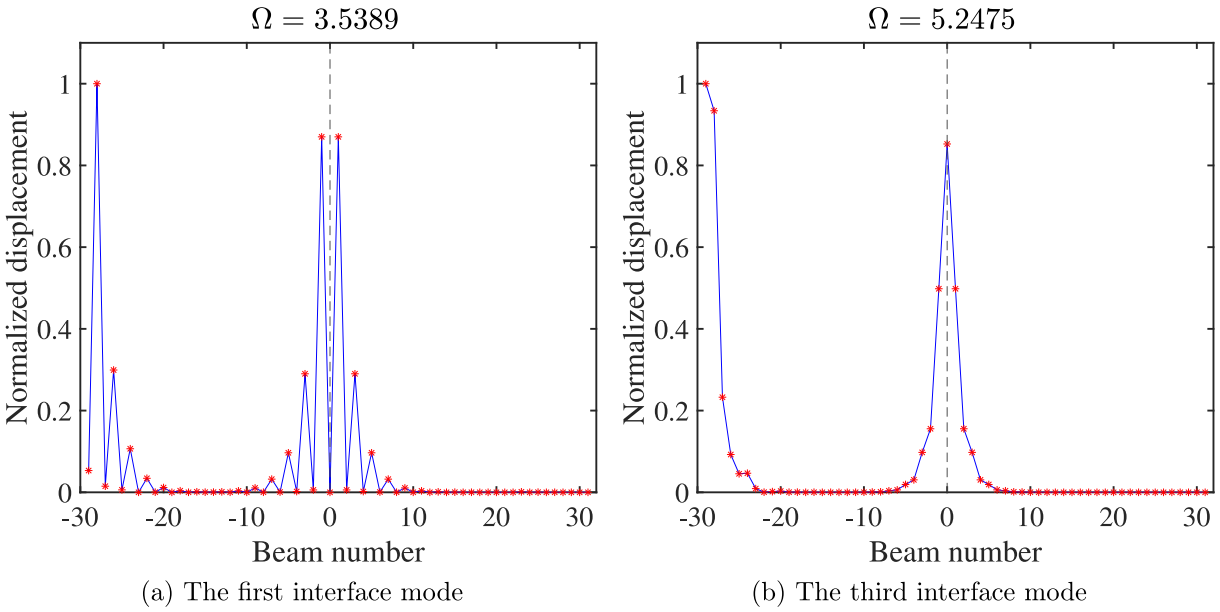

Fig. 11. Normalized steady-state displacement amplitudes of the beam array system with $n = 15$ unit cells on each side of the interface and the first beam $w_{b,-15}$ excited near the interface frequency for the values of parameters $\gamma = 0.5, d = 0.001$.

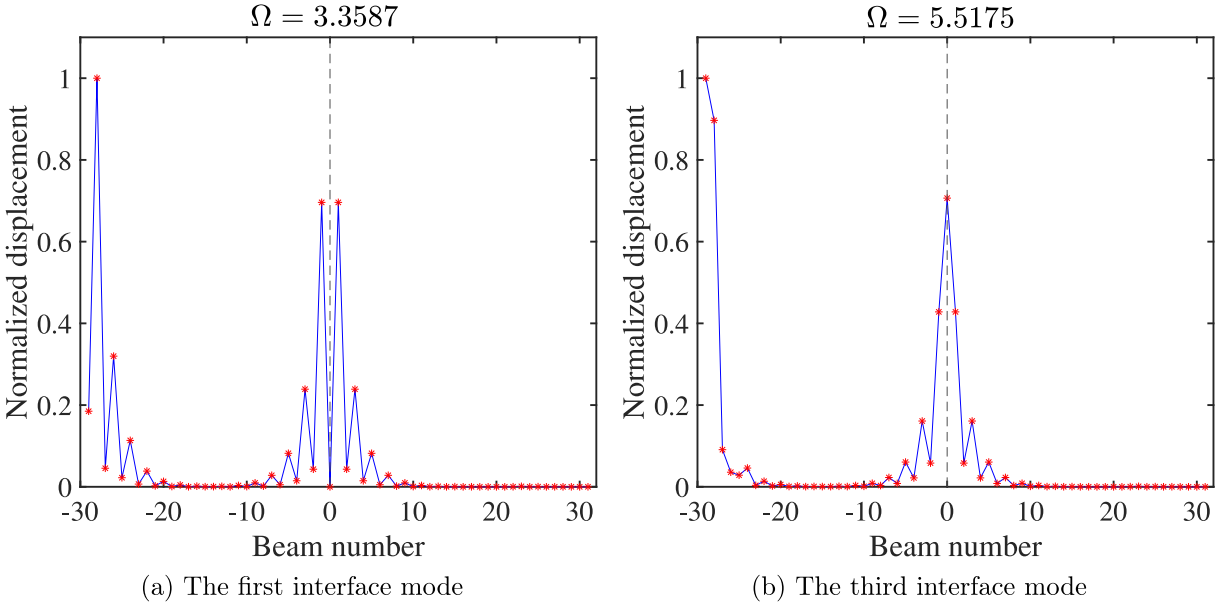

Fig. 12. Normalized steady-state displacement amplitudes of the beam array system with $n = 15$ unit cells on each side of the interface and the first beam $w_{b,-15}$ excited near the interface frequency for the values of parameters $\gamma = 0.5, d = 0.01$.

sponse function, and steady-state response amplitudes in space. Suitable numerical examples are given to illustrate the band inversion effect and the existence of interface modes in the proposed system. In this paper, we have made the following main contributions:

- In the beam array system without inerters we demonstrated the existence of multiple bands and interface modes mostly located within the narrow band gaps and localized at the interface between two sub-lattices.
- We examined the effect of defect mass introduced into the elastic beam array system and showed that existing interface mode frequencies are not affected by such changes. However, new defect modes localized at the place of defect mass emerge within the higher frequency band gaps for lower values of the defect mass and at both lower and higher frequency band gaps for the higher values of that mass.
- For the simple mass-spring-inerter chain we illustrated that the existing localized interface modes in the mass-spring chain can be shifted toward lower frequencies when introducing the inerters, while their symmetric properties are preserved.
- We revealed that multiple interface states in a beam array system with inerters at the interface can be tuned at both lower and higher frequency ranges by changing the inertance. More precisely, an increase of inertance leads to a decrease of lower interface frequencies while higher interface frequencies can migrate into bulk or even emerge at lower frequency band gaps.

This work shows how exploiting the inerters and their mass amplification effect can lead to tunable periodic mechanical structures ex-

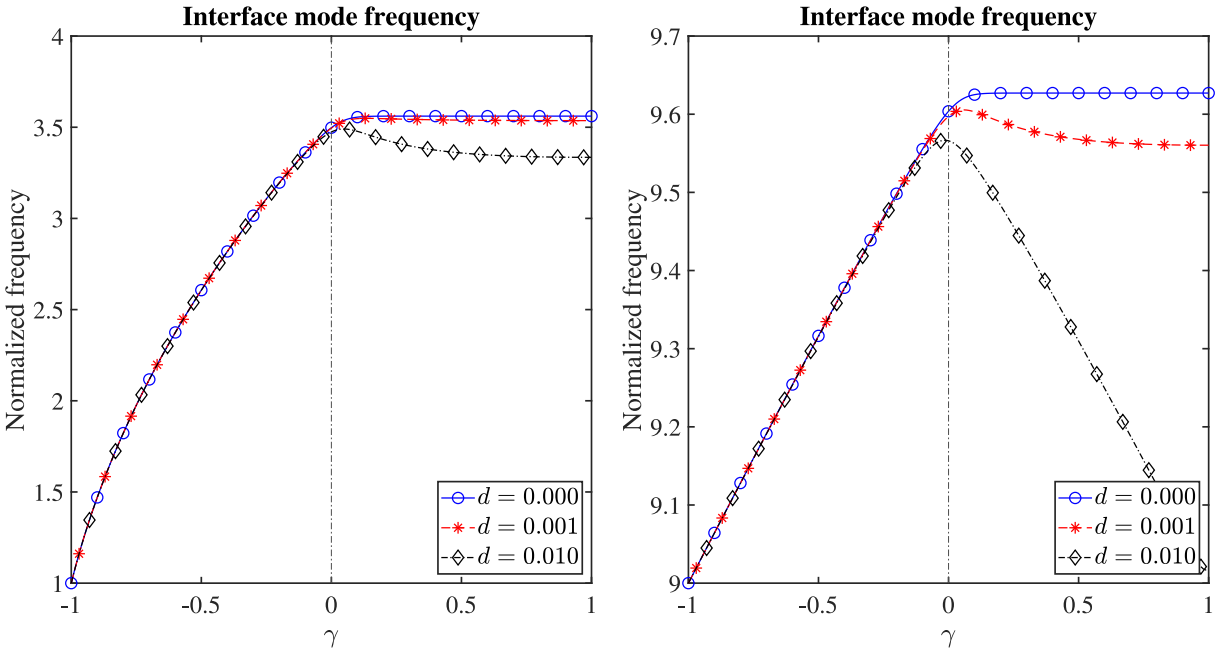

(a) The first interface mode (b) The fifth interface mode

Fig. 13. Interface frequencies of the beam array system with and without inerters for variations of γ and different values of inerter parameter d

hibiting localized modes at interfaces and showing high potential for application in future tunable engineering systems and devices.

Declaration of Competing Interest

The authors declare that they have no known competing financial interests or personal relationships that could have appeared to influence the work reported in this paper.

CRediT authorship contribution statement

Milan Cajić: Conceptualization, Methodology, Software, Writing - original draft. **Johan Christensen:** Writing - review & editing. **Sondipon Adhikari:** Project administration, Writing - review & editing.

Acknowledgements

This research is a part of a project that has received funding from the European Unions Horizon 2020 research and innovation programme under the Marie Skłodowska-Curie grant agreement No. 896942 (METASINK). M.C. acknowledges the partial support by the Ministry of Education, Science and Technological Development of the Republic of Serbia. J.C. acknowledges the support from the European Research Council (ERC) through the Starting Grant No. 714577 PHONOMETA and from the MINECO through a Ramón y Cajal grant (Grant No. RYC-2015-17156). This work has been also supported by Comunidad de Madrid (Spain) - multiannual agreement with UC3M ("Excelencia para el Profesorado Universitario" - EPUC3M14) - Fifth regional research plan 2016-2020.

Appendix A. Mode shape functions and matrix coefficients

In the Galerkin weighted residual method, the trial functions are considered as the weighting functions that need to satisfy the according boundary and orthogonality conditions. These requirements can be met by several types of functions, and in our case, the mode shape functions of a simply supported bare beam will be employed. Using this approximation method is especially important for the beams with attached concentrated masses since the exact mode shape function satisfying boundary conditions cannot be derived straightforwardly. If beams in the proposed beam array system are identical and have the same edge conditions, they can be approximated by the same trial functions. The mode shape functions of a bare simply supported beam can be expressed as

$$\phi_{(u,p)r} = \phi_r = \sqrt{\frac{2}{\rho A L}} \sin \beta_r x, \quad \beta_r = \frac{r\pi}{L}.$$

Above given function depends on a number of mode r while the relation between the bare beam natural frequency ω_r and dimensionless eigenvalue β_r is given as $\omega_r^2 = \beta_r^4 \frac{EI}{\rho A}$. The constant $\sqrt{\frac{2}{\rho A L}}$ is chosen such that it makes the trial functions mutually orthogonal and mass normalized, while the eigenvalue β_r is obtained as a solution of the well-known frequency equation of the simply supported beam.

To make the trial functions orthonormal with respect to the beam mass, the following orthogonality conditions are used

$$\int_0^L \rho A \phi_r(x) \phi_s(x) dx = \delta_{rs},$$

$$\int_0^L EI \phi_r(x) \phi_s(x) dx = \omega_r^2 \delta_{ks}, \quad r, s = 1, 2, ..., N.$$

where δ_{rs} is the Kronecker delta.

Mass $\mathbf{M}$ and stiffness $\mathbf{K}$ of dimension $(4n+1)N \times (4n+1)N$ are given as follows

$$\mathbf{M} = \begin{bmatrix} \mathbf{M}_1^{b,-n} & \mathbf{0} & ... & \mathbf{0} & \mathbf{0} & \mathbf{0} & \mathbf{0} & \mathbf{0} & \mathbf{0} & \mathbf{0} \\ \mathbf{0} & \mathbf{M}_2^{a,-n+1} & ... & \mathbf{0} & \mathbf{0} & \mathbf{0} & \mathbf{0} & \mathbf{0} & \mathbf{0} & \mathbf{0} \\ ... & ... & ... & \mathbf{0} & \mathbf{0} & \mathbf{0} & \mathbf{0} & \mathbf{0} & \mathbf{0} & \mathbf{0} \\ \mathbf{0} & \mathbf{0} & \mathbf{0} & \mathbf{M}_{2n-1}^{b,-1} & \mathbf{M}_{(d)}^{a,0} & \mathbf{0} & \mathbf{0} & \mathbf{0} & \mathbf{0} & \mathbf{0} \\ \mathbf{0} & \mathbf{0} & \mathbf{0} & \mathbf{M}_{(d)}^{b,-1} & \mathbf{M}_{2n}^{a,0} & \mathbf{M}_{(d)}^{b,0} & \mathbf{0} & \mathbf{0} & \mathbf{0} & \mathbf{0} \\ \mathbf{0} & \mathbf{0} & \mathbf{0} & \mathbf{0} & \mathbf{M}_{(d)}^{a,0} & \mathbf{M}_{2n+1}^{b,0} & \mathbf{0} & \mathbf{0} & \mathbf{0} & \mathbf{0} \\ \mathbf{0} & \mathbf{0} & \mathbf{0} & \mathbf{0} & \mathbf{0} & \mathbf{0} & \mathbf{M}_{2n+2}^{a,1} & \mathbf{0} & \mathbf{0} & \mathbf{0} \\ \mathbf{0} & \mathbf{0} & \mathbf{0} & \mathbf{0} & \mathbf{0} & \mathbf{0} & \mathbf{0} & ... & ... & ... \\ \mathbf{0} & \mathbf{0} & \mathbf{0} & \mathbf{0} & \mathbf{0} & \mathbf{0} & \mathbf{0} & ... & \mathbf{M}_{4n}^{a,n} & \mathbf{0} \\ \mathbf{0} & \mathbf{0} & \mathbf{0} & \mathbf{0} & \mathbf{0} & \mathbf{0} & \mathbf{0} & ... & \mathbf{0} & \mathbf{M}_{4n+1}^{b,n} \end{bmatrix},$$

$$\mathbf{K}=\begin{bmatrix}
\mathbf{K}_{1}^{b,-n} & \mathbf{K}_{(k_1)}^{a,-n+1} & \dots & \mathbf{0} & \mathbf{0} & \mathbf{0} & \mathbf{0} & \mathbf{0} & \mathbf{0} & \mathbf{0}\\
\mathbf{K}_{(k_1)}^{b,-n} & \mathbf{K}_{2}^{a,-n+1} & \dots & \mathbf{0} & \mathbf{0} & \mathbf{0} & \mathbf{0} & \mathbf{0} & \mathbf{0} & \mathbf{0}\\
\dots & \dots & \dots & \mathbf{K}_{(k_2)}^{b,-1} & \mathbf{0} & \mathbf{0} & \mathbf{0} & \mathbf{0} & \mathbf{0} & \mathbf{0}\\
\mathbf{0} & \mathbf{0} & \mathbf{K}_{(k_2)}^{a,-1} & \mathbf{K}_{2n-1}^{b,-1} & \mathbf{K}_{(k_1)}^{a,0} & \mathbf{0} & \mathbf{0} & \mathbf{0} & \mathbf{0} & \mathbf{0}\\
\mathbf{0} & \mathbf{0} & \mathbf{0} & \mathbf{K}_{(k_1)}^{b,-1} & \mathbf{K}_{2n}^{a,0} & \mathbf{K}_{(k_1)}^{b,0} & \mathbf{0} & \mathbf{0} & \mathbf{0} & \mathbf{0}\\
\mathbf{0} & \mathbf{0} & \mathbf{0} & \mathbf{0} & \mathbf{K}_{(k_1)}^{a,0} & \mathbf{K}_{2n+1}^{b,0} & \mathbf{K}_{(k_2)}^{a,1} & \mathbf{0} & \mathbf{0} & \mathbf{0}\\
\mathbf{0} & \mathbf{0} & \mathbf{0} & \mathbf{0} & \mathbf{0} & \mathbf{K}_{(k_2)}^{b,0} & \mathbf{K}_{2n+2}^{a,1} & \mathbf{K}_{(k_1)}^{b,1} & \mathbf{0} & \mathbf{0}\\
\mathbf{0} & \mathbf{0} & \mathbf{0} & \mathbf{0} & \mathbf{0} & \mathbf{0} & \mathbf{K}_{(k_1)}^{a,1} & \dots & \dots & \dots\\
\mathbf{0} & \mathbf{0} & \mathbf{0} & \mathbf{0} & \mathbf{0} & \mathbf{0} & \mathbf{0} & \dots & \mathbf{K}_{4n}^{a,n} & \mathbf{K}_{(k_1)}^{b,n}\\
\mathbf{0} & \mathbf{0} & \mathbf{0} & \mathbf{0} & \mathbf{0} & \mathbf{0} & \mathbf{0} & \dots & \mathbf{K}_{(k_1)}^{a,n} & \mathbf{K}_{4n+1}^{b,n}
\end{bmatrix},$$

while vector $\mathbf{q}$ is given as

$$\overline{\mathbf{q}}=\begin{bmatrix}\mathbf{q}_{1}^{b,-n} & \mathbf{q}_{2}^{b,-n+1} & \dots & \mathbf{q}_{2n-1}^{b,-1} & \mathbf{q}_{2n}^{a,0} & \mathbf{q}_{2n+1}^{b,0} & \mathbf{q}_{2n+2}^{a,1} & \dots & \mathbf{q}_{4n}^{a,n} & \mathbf{q}_{4n+1}^{b,n}\end{bmatrix}^{T}.$$

By taking into account adopted mode shapes and orthogonality conditions, one can determine the coefficients of the above global mass matrix by defining the $N\times N$ diagonal submatrices calculated as

$$M_{(i)rs}^{u,p}=\rho A\int_0^L\phi_r\phi_s dx=\begin{cases}1, & \text{for } r=s,\\ 0, & \text{for } r\neq s,\end{cases}\qquad i=1,2,...,4n+1.$$

If we consider that concentrated masses are attaches to beam denoted with b in the p-th unit cell, then the corresponding diagonal submatrix is given as

$$M_{(i)rs}^{u,p}=\int_0^L(\rho A+\sum_{\xi=1}^{\Xi}m_\xi\delta(x-\sigma_\xi))\phi_r\phi_s dx=\begin{cases}1+\sum_{\xi=1}^{\Xi}m_\xi\phi_r^2(\sigma_\xi), & \text{for } r=s,\\ 0, & \text{for } r\neq s.\end{cases}$$

Further, diagonal submatrices related to the interface beam connected with adjacent beams through inerters and springs are given as

$$M_{(i)rs}^{b,-1}=M_{(i)rs}^{b,0}=(\rho A+d)\int_0^L\phi_r\phi_s dx=\begin{cases}1+\frac{d}{\rho A}, & \text{for } r=s,\\ 0, & \text{for } r\neq s,\end{cases}\qquad i=2n-1,2n+1,$$

$$M_{(i)rs}^{a,0}=(\rho A+2d)\int_0^L\phi_r\phi_s dx=\begin{cases}1+\frac{2d}{\rho A}, & \text{for } r=s,\\ 0, & \text{for } r\neq s,\end{cases}\qquad i=2n,$$

and super and sub diagonal submatricies given as

$$M_{(d)rs}^{a,0}=M_{(d)rs}^{b,0}=M_{(d)rs}^{b,-1}=-d\int_0^L\phi_r\phi_s dx=\begin{cases}-\frac{d}{\rho A}, & \text{for } r=s,\\ 0, & \text{for } r\neq s,\end{cases}.$$

Similarly, diagonal submatricies of the global stiffness matrix can be calculated as

$$\begin{aligned}K_{(i)rs}^{u,p}&=EI\int_0^L\phi_{(u,p)r}''''\phi_{(u,p)s}dx+(k_1+k_2)\int_0^L\phi_{(u,p)r}\phi_{(u,p)s}dx\\&=\begin{cases}\tilde{\omega}_r^2+\frac{k_1+k_2}{\rho A}, & \text{for } r=s,\\ 0, & \text{for } r\neq s,\end{cases}\qquad i=1,2,...,4n+1.\end{aligned}$$

and super and sub diagonal submatricies as

$$K_{(k_1)rs}^{u,p}=-k_1\int_0^L\phi_{(u,p)r}\phi_{(u,p)s}dx=\begin{cases}-\frac{k_1}{\rho A}, & \text{for } r=s.\\ 0, & \text{for } r\neq s.\end{cases}$$

$$K_{(k_2)rs}^{u,p}=-k_2\int_0^L\phi_{(u,p)r}\phi_{(u,p)s}dx=\begin{cases}-\frac{k_2}{\rho A}, & \text{for } r=s.\\ 0, & \text{for } r\neq s.\end{cases}$$

Appendix B. Matrix coefficients for the band structure

Dimension of mass $\mathbf{M}_p$ and stiffness $\mathbf{K}_p$ matrices in Eq. (13) is $2N\times 2N$, which depends on the number of adopted terms in the Galerkin approximation. Following the same procedure as above, and adopting the corresponding mode shapes and orthogonality conditions, the elements of the mass and stiffness matrix are determined as

$$M_{(1)rs}^{a,p}=M_{(2)ks}^{b,p}=\rho A\int_0^L\phi_{(u,p)r}\phi_{(u,p)s}dx=\begin{cases}1, & \text{for } r=s.\\ 0, & \text{for } r\neq s.\end{cases},$$

$$\begin{aligned}K_{(11)rs}^{a,p}&=K_{(22)rs}^{b,p}=EI\int_0^L\phi_{(u,p)r}''''\phi_{(u,p)s}dx+(k_1+k_2)\int_0^L\phi_{(u,p)r}\phi_{(u,p)s}dx\\&=\begin{cases}\tilde{\omega}_r^2+\frac{k_1+k_2}{\rho A}, & \text{for } r=s.\\ 0, & \text{for } r\neq s.\end{cases}\end{aligned}$$

$$K_{(12)rs}^{a,p}=-(k_1+k_2e^{-j\mu a})\int_0^L\phi_{(u,p)r}\phi_{(u,p)s}dx=\begin{cases}\frac{-k_1-k_2e^{-j\mu a}}{\rho A}, & \text{for } r=s.\\ 0, & \text{for } r\neq s.\end{cases}$$

$$K_{(21)rs}^{a,p}=-(k_1+k_2e^{j\mu a})\int_0^L\phi_{(u,p)r}\phi_{(u,p)s}dx=\begin{cases}\frac{-k_1-k_2e^{j\mu a}}{\rho A}, & \text{for } r=s.\\ 0, & \text{for } r\neq s.\end{cases}$$

Appendix C. Mass-spring-inerter chain

Let us consider the mass-spring-inerter system with a unit cell composed of identical masses connected through springs with stiffnesses $k_1^s=\kappa(1+\gamma)$ and $k_1^s=\kappa(1-\gamma)$ and inerters with the same inertia amplification property d_I. If this mass-spring-inerter chain contains two sublattices of unit cells that are inverted copies of each other (see Fig. C.14), the governing equation for the free vibration of the interface mass $y_{a,0}$ is given as

$$m\ddot{y}_{a,0}+2d_I\ddot{y}_{a,0}+2k_1^sy_{a,0}-k_1^sy_{b,0}-k_1^sy_{b,-1}-d_I\ddot{y}_{b,0}-d_I\ddot{y}_{b,-1}=0,$$

In the similar manner, one can obtain the equations for a unit cell p of the sub-lattice I on the left side of the interface as

$$m\ddot{y}_{a,p}+d_I(\ddot{y}_{a,p}-\ddot{y}_{b,p})+d_I(\ddot{y}_{a,p}-\ddot{y}_{b,p-1})+k_2^s(y_{a,p}-y_{b,p})+k_1^s(y_{a,p}-y_{b,p-1})=0,$$

$$m\ddot{y}_{b,p}+d_I(y_{b,p}-y_{a,p})+d_I(y_{b,p}-y_{a,p+1})+k_2^s(y_{b,p}-y_{a,p})+k_1^s(y_{b,p}-y_{a,p+1})=0,$$

and for the sub-lattice II on the right side of the interface as

$$m\ddot{y}_{a,p}+d_I(\ddot{y}_{a,p}-\ddot{y}_{b,p})+d_I(\ddot{y}_{a,p}-\ddot{y}_{b,p-1})+k_1^s(y_{a,p}-y_{b,p})+k_2^s(y_{a,p}-y_{b,p-1})=0,$$

$$m\ddot{y}_{b,p}+d_I(\ddot{y}_{b,p}-\ddot{y}_{a,p})+d_I(\ddot{y}_{b,p}-\ddot{y}_{a,p+1})+k_1^s(y_{b,p}-y_{a,p})+k_2^s(y_{b,p}-y_{a,p+1})=0.$$

If we introduce the non-dimensional time scale $\tau=(\sqrt{\kappa/m})t$, then the dimensionless parameters related to the inertance and stiffness are given as $\tilde{d}=d_I/m$ and $\tilde{k}_1^s=1+\gamma$, $\tilde{k}_2^s=1-\gamma$, respectively. For the chain with a finite number of unit cells and forced response of the mass-spring-inerter system one can write the above equations in matrix form as $\mathbf{M}^I\ddot{\mathbf{y}}(\tau)+\mathbf{K}^s\mathbf{y}(\tau)=\mathbf{f}(\tau)$, where $\mathbf{f}(\tau)=\mathbf{f}^se^{j\Omega\tau}$, with Ω is denoting the frequency normalized with the reference frequency $\sqrt{\kappa/m}$. By imposing the solution of the form $\mathbf{y}(\tau)=\overline{\mathbf{y}}e^{j\Omega\tau}$, the governing equation reduces to

$$\left(\mathbf{K}^s-\Omega^2\mathbf{M}^I\right)\overline{\mathbf{y}}=\mathbf{f}.$$

By taking that $\mathbf{f}=0$, one obtains the eigenvalue problem whose solution gives natural frequencies Ω of the proposed mass-spring-inerter chain system. For the finite number of n unit cells on each side of the interface and fixed-free chain, where the first mass on the left side $y_{b,-n}$ is fixed to the base, the elements of the mass matrix $\mathbf{M}^I$ and stiffness $\mathbf{K}^s$ matrix of dimension $(4n+1)\times(4n+1)$ are given as

$$\mathbf{M}^I=\begin{bmatrix}
1+2\tilde{d} & -\tilde{d} & \dots & 0 & 0 & 0 & 0 & 0 & 0 & 0\\
-\tilde{d} & 1+2\tilde{d} & \dots & 0 & 0 & 0 & 0 & 0 & 0 & 0\\
\dots & \dots & \dots & -\tilde{d} & 0 & 0 & 0 & 0 & 0 & 0\\
0 & 0 & -\tilde{d} & 1+2\tilde{d} & -\tilde{d} & 0 & 0 & 0 & 0 & 0\\
0 & 0 & 0 & -\tilde{d} & 1+2\tilde{d} & -\tilde{d} & 0 & 0 & 0 & 0\\
0 & 0 & 0 & 0 & -\tilde{d} & 1+2\tilde{d} & -\tilde{d} & 0 & 0 & 0\\
0 & 0 & 0 & 0 & 0 & -\tilde{d} & 1+2\tilde{d} & -\tilde{d} & 0 & 0\\
0 & 0 & 0 & 0 & 0 & 0 & -\tilde{d} & \dots & \dots & \dots\\
0 & 0 & 0 & 0 & 0 & 0 & 0 & \dots & 1+2\tilde{d} & -\tilde{d}\\
0 & 0 & 0 & 0 & 0 & 0 & 0 & \dots & -\tilde{d} & 1+\tilde{d}
\end{bmatrix},$$

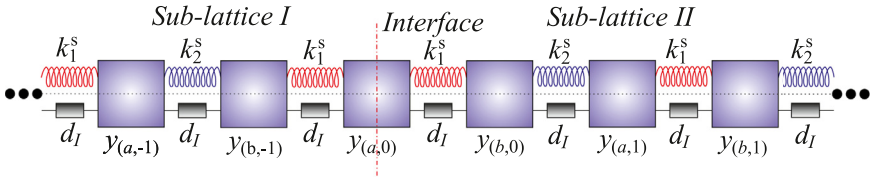

Fig. C.14. Illustration of the mass-spring-inerter chain system.

$$\mathbf{K}^s = \begin{bmatrix} \tilde{k}_1^s + \tilde{k}_2^s & -\tilde{k}_1^s & \dots & 0 & 0 & 0 & 0 & 0 & 0 & 0 \\ -\tilde{k}_1^s & \tilde{k}_1^s + \tilde{k}_2^s & \dots & 0 & 0 & 0 & 0 & 0 & 0 & 0 \\ \dots & \dots & \dots & -\tilde{k}_2^s & 0 & 0 & 0 & 0 & 0 & 0 \\ 0 & 0 & -\tilde{k}_2^s & \tilde{k}_1^s + \tilde{k}_2^s & -\tilde{k}_1^s & 0 & 0 & 0 & 0 & 0 \\ 0 & 0 & 0 & -\tilde{k}_1^s & 2\tilde{k}_1^s & -\tilde{k}_1^s & 0 & 0 & 0 & 0 \\ 0 & 0 & 0 & 0 & -\tilde{k}_1^s & \tilde{k}_1^s + \tilde{k}_2^s & -\tilde{k}_2^s & 0 & 0 & 0 \\ 0 & 0 & 0 & 0 & 0 & -\tilde{k}_2^s & \tilde{k}_1^s + \tilde{k}_2^s & -\tilde{k}_1^s & 0 & 0 \\ 0 & 0 & 0 & 0 & 0 & 0 & -\tilde{k}_1^s & \dots & \dots & \dots \\ 0 & 0 & 0 & 0 & 0 & 0 & 0 & \dots & \tilde{k}_1^s + \tilde{k}_2^s & -\tilde{k}_1^s \\ 0 & 0 & 0 & 0 & 0 & 0 & 0 & \dots & -\tilde{k}_1^s & \tilde{k}_1^s \end{bmatrix},$$

References

[1] Bordiga G, Cabras L, Bigoni D, Piccolroaz A. Free and forced wave propagation in a rayleigh-beam grid: flat bands, dirac cones, and vibration localization vs isotropization. Int J Solids Struct 2019;161:64–81.
[2] Wang P, Lu L, Bertoldi K. Topological phononic crystals with one-way elastic edge waves. PhysRevLett 2015;115(10):104302.
[3] Qi X-L, Zhang S-C. The quantum spin hall effect and topological insulators. arXiv preprint arXiv:10011602 2010.
[4] Moore JE. The birth of topological insulators. Nature 2010;464(7286):194–8.
[5] Lu L, Joannopoulos JD, Soljačić M. Topological photonics. NatPhotonics 2014;8(11):821–9.
[6] Wang H, Liu D, Fang W, Lin S, Liu Y, Liang Y. Tunable topological interface states in one-dimensional extended granular crystals. Int J Mech Sci 2020;176:105549.
[7] Huang Y, Huang Y, Chen W, Bao R. Flexible manipulation of topologically protected waves in one-dimensional soft periodic plates. Int J Mech Sci 2020;170:105348.
[8] Hasan MA, Calderin L, Lucas P, Runge K, Deymier PA. Spectral analysis of amplitudes and phases of elastic waves: application to topological elasticity. J Acoust Soc Am 2019;146(1):748–66.
[9] Zak J. Berrys phase for energy bands in solids. PhysRevLett 1989;62(23):2747.
[10] Hasan MA, Calderin L, Lucas P, Runge K, Deymier PA. Geometric phase invariance in spatiotemporal modulated elastic system. J Sound Vib 2019;459:114843.
[11] Hasan MZ, Kane CL. Colloquium: topological insulators. RevModPhys 2010;82(4):3045.
[12] Liu Y, Chen X, Xu Y. Topological phononics: from fundamental models to real materials. Adv Funct Mater 2020;30(8):1904784.
[13] He C, Ni X, Ge H, Sun X-C, Chen Y-B, Lu M-H, et al. Acoustic topological insulator and robust one-way sound transport. NatPhys 2016;12(12):1124–9.
[14] Zhang Z, Wei Q, Cheng Y, Zhang T, Wu D, Liu X. Topological creation of acoustic pseudospin multipoles in a flow-free symmetry-broken metamaterial lattice. PhysRevLett 2017;118(8):084303.
[15] Zhang X, Xiao M, Cheng Y, Lu M, Christensen J. Topological sound. Commun Phys 2018;1:1–13.
[16] Chen Y, Liu X, Hu G. Topological phase transition in mechanical honeycomb lattice. J Mech Phys Solids 2019;122:54–68.
[17] Wang W, Bonello B, Djafari-Rouhani B, Pennec Y. Topological valley, pseudospin, and pseudospin-valley protected edge states in symmetric pillared phononic crystals. Phys Rev B 2019;100(14):140101.
[18] Fan H, Xia B, Tong L, Zheng S, Yu D. Elastic higher-order topological insulator with topologically protected corner states. PhysRevLett 2019;122(20):204301.
[19] Xiao M, Zhang Z, Chan CT. Surface impedance and bulk band geometric phases in one-dimensional systems. Phys Rev X 2014;4(2):021017.
[20] Choi KH, Ling C, Lee K, Tsang YH, Fung KH. Simultaneous multi-frequency topological edge modes between one-dimensional photonic crystals. OptLett 2016;41(7):1644–7.
[21] Zhang Z, Cheng Y, Liu X, Christensen J. Subwavelength multiple topological interface states in one-dimensional labyrinthine acoustic metamaterials. Phys Rev B 2019;99(22):224104.
[22] Liu Y, Jin L, Wang H, Liu D, Liang Y. Topological interface states in translational metamaterials for sub-wavelength in-plane waves. Int J Mech Sci 2021:106308.
[23] Al Ba'ba'a H, Nouh M, Singh T. Dispersion and topological characteristics of permutative polyatomic phononic crystals. Proc R Soc A 2019;475(2226):20190022.
[24] Chen H, Nassar H, Huang G. A study of topological effects in 1d and 2d mechanical lattices. J Mech Phys Solids 2018;117:22–36.
[25] Marques A, Dias R. Generalization of zak's phase for lattice models with non-centered inversion symmetry axis. arXiv preprint arXiv:170706162 2017.
[26] Wang H-X, Guo G-Y, Jiang J-H. Band topology in classical waves: Wilson-loop approach to topological numbers and fragile topology. N J Phys 2019;21(9):093029.
[27] Rudner MS, Levin M, Levitov LS. Survival, decay, and topological protection in non-hermitian quantum transport. arXiv preprint arXiv:160507652 2016.
[28] Chen H, Yao L, Nassar H, Huang G. Mechanical quantum hall effect in time-modulated elastic materials. Phys Rev Appl 2019;11(4):044029.
[29] Zhou W, Lim C, et al. Topological edge modeling and localization of protected interface modes in 1d phononic crystals for longitudinal and bending elastic waves. Int J Mech Sci 2019;159:359–72.
[30] Mousavi SH, Khanikaev AB, Wang Z. Topologically protected elastic waves in phononic metamaterials. NatCommun 2015;6(1):1–7.
[31] Khanikaev AB, Fleury R, Mousavi SH, Alu A. Topologically robust sound propagation in an angular-momentum-biased graphene-like resonator lattice. NatCommun 2015;6(1):1–7.
[32] Zhang Z, Tian Y, Cheng Y, Liu X, Christensen J. Experimental verification of acoustic pseudospin multipoles in a symmetry-broken snowflakelike topological insulator. Phys Rev B 2017;96(24):241306.
[33] Pal RK, Ruzzene M. Edge waves in plates with resonators: an elastic analogue of the quantum valley hall effect. N J Phys 2017;19(2):025001.
[34] Pal RK, Vila J, Leamy M, Ruzzene M. Amplitude-dependent topological edge states in nonlinear phononic lattices. Phys Rev E 2018;97(3):032209.
[35] Yin J, Ruzzene M, Wen J, Yu D, Cai L, Yue L. Band transition and topological interface modes in 1d elastic phononic crystals. SciRep 2018;8(1):1–10.
[36] Fan L, He Y, Zhao X, Chen X-a. Subwavelength and broadband tunable topological interface state for flexural wave in one-dimensional locally resonant phononic crystal. J Appl Phys 2020;127(23):235106.
[37] Huang H, Chen J, Huo S. Simultaneous topological Bragg and locally resonant edge modes of shear horizontal guided wave in one-dimensional structure. J Phys D 2017;50(27):275102.
[38] Chen J, Huang H, Huo S, Tan Z, Xie X, Cheng J, et al. Self-ordering induces multiple topological transitions for in-plane bulk waves in solid phononic crystals. Phys Rev B 2018;98(1):014302.
[39] Deymier P, Runge K, Hasan MA. Exponentially complex nonseparable states in planar arrays of nonlinearly coupled one-dimensional elastic waveguides. J Phys Commun 2020;4(8):085018.
[40] Liu J, Guo H, Wang T. A review of acoustic metamaterials and phononic crystals. Crystals 2020;10(4):305.
[41] Jo S-H, Yoon H, Shin YC, Youn BD. An analytical model of a phononic crystal with a piezoelectric defect for energy harvesting using an electroelastically coupled transfer matrix. Int J Mech Sci 2020;193:106160.
[42] Nieves M, Brun M. Dynamic characterization of a periodic microstructured flexural system with rotational inertia. Philos Trans R Soc A 2019;377(2156):20190113.
[43] Rosa MI, Pal RK, Arruda JR, Ruzzene M. Edge states and topological pumping in spatially modulated elastic lattices. PhysRevLett 2019;123(3):034301.
[44] Ning L, Wang Y-Z, Wang Y-S. Active control cloak of the elastic wave metamaterial. Int J Solids Struct 2020;202:126–35.
[45] Li G-H, Ma T-X, Wang Y-Z, Wang Y-S. Active control on topological immunity of elastic wave metamaterials. SciRep 2020;10(1):1–8.
[46] Avila-Pozos O, Movchan A, Sorokin S. Propagation of elastic waves along interfaces in layered beams. In: IUTAM Symposium on Asymptotics, Singularities and Homogenisation in Problems of Mechanics. Springer; 2003. p. 53–61.
[47] Hajarolasvadi S, Elbanna AE. Dynamics of metamaterial beams consisting of periodically-coupled parallel flexural elements: a theoretical study. J Phys D 2019;52(31):315101.
[48] Paunović S, Cajić M, Karličić D, Mijalković M. Dynamics of fractional-order multi--beam mass system excited by base motion. Appli Math Model 2020;80:702–23.
[49] Karličić D, Cajić M, Adhikari S, Kozić P, Murmu T. Vibrating nonlocal multi–nanoplate system under inplane magnetic field. Eur J Mech-A/Solids 2017;64:29–45.
[50] Karličić D, Cajić M, Paunović S, Adhikari S. Bloch waves in an array of elastically connected periodic slender structures. Mech Syst Signal Process 2021;155:107591.
[51] Hasan MA, Calderin L, Lata T, Lucas P, Runge K, Deymier PA. Directional elastic pseudospin and nonseparability of directional and spatial degrees of freedom in parallel arrays of coupled waveguides. Appl Sci 2020;10(9):3202.
[52] Deymier P, Hasan M, Runge K. Navigating the hilbert space of nonseparable elastic states in arrays of periodically coupled one-dimensional waveguides. AIP Adv 2020;10(9):095105.
[53] Chen Q, Zhao Z, Xia Y, Pan C, Luo H, Zhang R. Comfort based floor design employing tuned inerter mass system. J Sound Vib 2019;458:143–57.
[54] Zhao Z, Chen Q, Zhang R, Jiang Y, Xia Y. Interaction of two adjacent structures coupled by inerter-based system considering soil conditions. J Earthq Eng 2020:1–21.
[55] Zhao Z, Zhang R, Pan C, Chen Q, Jiang Y. Input energy reduction principle of structures with generic tuned mass damper inerter. Struct Control Health Monit 2021;28(1):e2644.
[56] Smith MC. The inerter: a retrospective. Annu Rev Control Robot AutonSyst 2020;3:361–91.
[57] Arakaki T, Kuroda H, Arima F, Inoue Y, Baba K. Development of seismic devices applied to ball screw: part 1 basic performance test of rd-series. AIJ J Technol Des 1999;5(8):239–44.

[58] Smith MC. Synthesis of mechanical networks: the inerter. IEEE TransAutomControl 2002;47(10):1648–62.
[59] Smith MC, Force-controlling mechanical device. US Patent US7316303B2, 2008.
[60] Papageorgiou C, Houghton NE, Smith MC. Experimental testing and analysis of inerter devices. JDynSystMeasureControl 2009;131(1).
[61] Gonzalez-Buelga A, Clare L, Neild S, Jiang J, Inman D. An electromagnetic inerter-based vibration suppression device. Smart Mater Struct 2015;24(5):055015.
[62] Simonovic J. Non-linear dynamics of a double-plate system coupled by a layer with viscoelastic and inertia properties. Sci Tech Rev 2012;62(1):40–54.
[63] Ikago K, Saito K, Inoue N. Seismic control of single-degree-of-freedom structure using tuned viscous mass damper. Earthq Eng Struct Dyn 2012;41(3):453–74.
[64] Chen MZ, Hu Y, Huang L, Chen G. Influence of inerter on natural frequencies of vibration systems. J Sound Vib 2014;333(7):1874–87.
[65] Hu Y, Chen MZ, Smith MC. Natural frequency assignment for mass-chain systems with inerters. Mech Syst Signal Process 2018;108:126–39.
[66] Jin X, Chen MZ, Huang Z. Minimization of the beam response using inerter-based passive vibration control configurations. Int J Mech Sci 2016;119:80–7.
[67] Simonović J. Influence of rolling visco-elastic coupling on non-linear dynamics of double plates system. Iran J Sci TechnolTrans Mech Eng 2015;39(M1 +):163–73.
[68] Al Ba'ba'a H, DePauw D, Singh T, Nouh M. Dispersion transitions and pole-zero characteristics of finite inertially amplified acoustic metamaterials. J Appl Phys 2018;123(10):105106.
[69] Brzeski P, Kapitaniak T, Perlikowski P. Novel type of tuned mass damper with inerter which enables changes of inertance. J Sound Vib 2015;349:56–66.
[70] Krenk S, Høgsberg J. Tuned resonant mass or inerter-based absorbers: unified calibration with quasi-dynamic flexibility and inertia correction. Proc R Soc A 2016;472(2185):20150718.
[71] Kelly SG. Free and forced vibrations of elastically connected structures. Adv Acoust Vib 2010;2010.
[72] Shaat M. Nonreciprocal elasticity. arXiv preprint arXiv:200413510 2020.